Report No.
SAIC-TN-96040

LDEF Satellite Radiation Analyses

Science Applications International Corporation
An Employee-Owned Company

by

T. W. Armstrong
B. L. Colborn

Work Performed for

NASA Marshall Space Flight Center
Space Sciences Laboratory, Astrophysics Branch
Huntsville, AL

FINAL REPORT
Contract No. NAS8 - 39386

March 1996

Route 2, Prospect, Tennessee 38477

Table of Contents

1. Introduction and Summary

This report covers work performed by Science Applications International Corporation (SAIC) under contract NAS8-39386 from the NASA Marshall Space Flight Center entitled "LDEF Satellite Radiation Analyses". The basic objective of the study was to evaluate the accuracy of present models and computational methods for defining the ionizing radiation environment for spacecraft in low Earth orbit (LEO) by making comparisons with radiation measurements made on the Long Duration Exposure Facility (LDEF) satellite, which was recovered after almost six years in space.

1.1 Scope

The emphasis of the work here is on predictions and comparisons with LDEF measurements of induced radioactivity and linear energy transfer (LET) measurements. These model/data comparisons have been used to evaluate the accuracy of current models for predicting the flux and directionality of trapped protons for LEO missions.

1.2 Publications

Most of the results from work on this contract have been described previously in publications and presentations. These are summarized in Table 1 together with earlier SAIC publications on SAIC analyses related to LDEF.

1.3 Organization of Report and Major Findings

LDEF 3-D Mass Model : Work on developing a 3-D mass model of the LDEF spacecraft and experiment payloads for radiation calculations was performed previous to the current contract effort. However, some additional work on verifying the model was performed under the present contract as discussed in Sec. 2.

Trapped Proton Anisotropy: Calculations of the activation of LDEF tray clamps and comparisons with measurements are given in Sec 3. These LDEF measurements are used to check model predictions of the trapped proton anisotropy.

Trapped Proton Flux: Model predictions of the trapped proton flux have been used to compare with several different types of LDEF data (absorbed dose, several sets of activation data, and fission foil measurements), as summarized in Sec. 4. Details of the model calculations and

Table 1. References by subject area to publications containing SAIC contributions to LDEF model predictions and data comparisons. (References are given in Sec. 6.)

Subject Area	LDEF Post-Retrieval Symposia Papers			Conference Papers	Journal Articles	SAIC Reports
	1st Symposium	2nd Symposium	3rd Symposium			
Activation						
Experiments						
Metal Samples			9*		2*	26*
Fission Foils			11*			
Spacecraft Components						
Tray Clamps	19		9*		2*, 6	26*
Trunnions	19				2*	
Cross Sections						27*
Trapped Protons	19	13,17	9*		3*,6	
		13				
Neutrons			11*			
Cosmic Rays					7	
Linear Energy Transfer (LET)		16	10*		3*	26*
Radiation Exposure Predictions	19, 21	13, 18	10*		5*	
3-D Spacecraft/Exp. Mass Model	20	15			4*	29
Pre-Recovery Predictions					7,8	30
Overviews/Summaries		14	12*	22*,23*,24,25	1*,6	26*,28

* Work performed under contract effort reported here.

comparisons with activation measurements for metal samples placed on LDEF are included as Appendix A.

LET Spectra: Section 5 summarizes model calculations and comparisons with LET spectra measured on LDEF. The emphasis of this work is on Monte Carlo calculations and LDEF data comparisons for the high-LET part of the spectrum due to recoil particles from proton-nucleus interactions (target fragments). Results of additional LET calculations are given in Appendix B.

References: A bibliography of SAIC contributions to LDEF radiation analyses and model validation calculations is given in Sec. 6; other references are given in Sec 7.

2. LDEF Mass Model Verification

Work on development of a detailed, three-dimensional mass model of LDEF for radiation analyses has been described previously /15,20,29/. Under the present effort an additional verification of the model was made as described below.

The LDEF mass model was developed using combinatorial geometry methodology. While graphics programs are available that use geometry model descriptions in this format to aid in de-bugging, and such a graphic program was used to help de-bug the LDEF model, the graphics programs that can be interfaced with combinatorial geometry models are generally of limited capability. Therefore, the combinatorial geometry description of LDEF was translated into a different format so that it could be used as input to the CADrays program /31/, which is an extension of the AutoCAD graphics package and was written by SAIC (for NASA/MSFC) for modeling the International Space Station. Pictures of the CADrays version of the LDEF model are shown in Fig. 1.

Using the CADrays version of LDEF, some "interferences" were found where geometric bodies overlapped in error. However, the overlaps were few in number and due to small dimensioning errors, so previous radiation calculations using the combinatorial geometry model were not affected. The CADrays program also provides the capability of computing the mass of the modeled geometric bodies. The calculated masses for geometric bodies comprising the LDEF model differed, at most, by a few percent from the expected body masses.

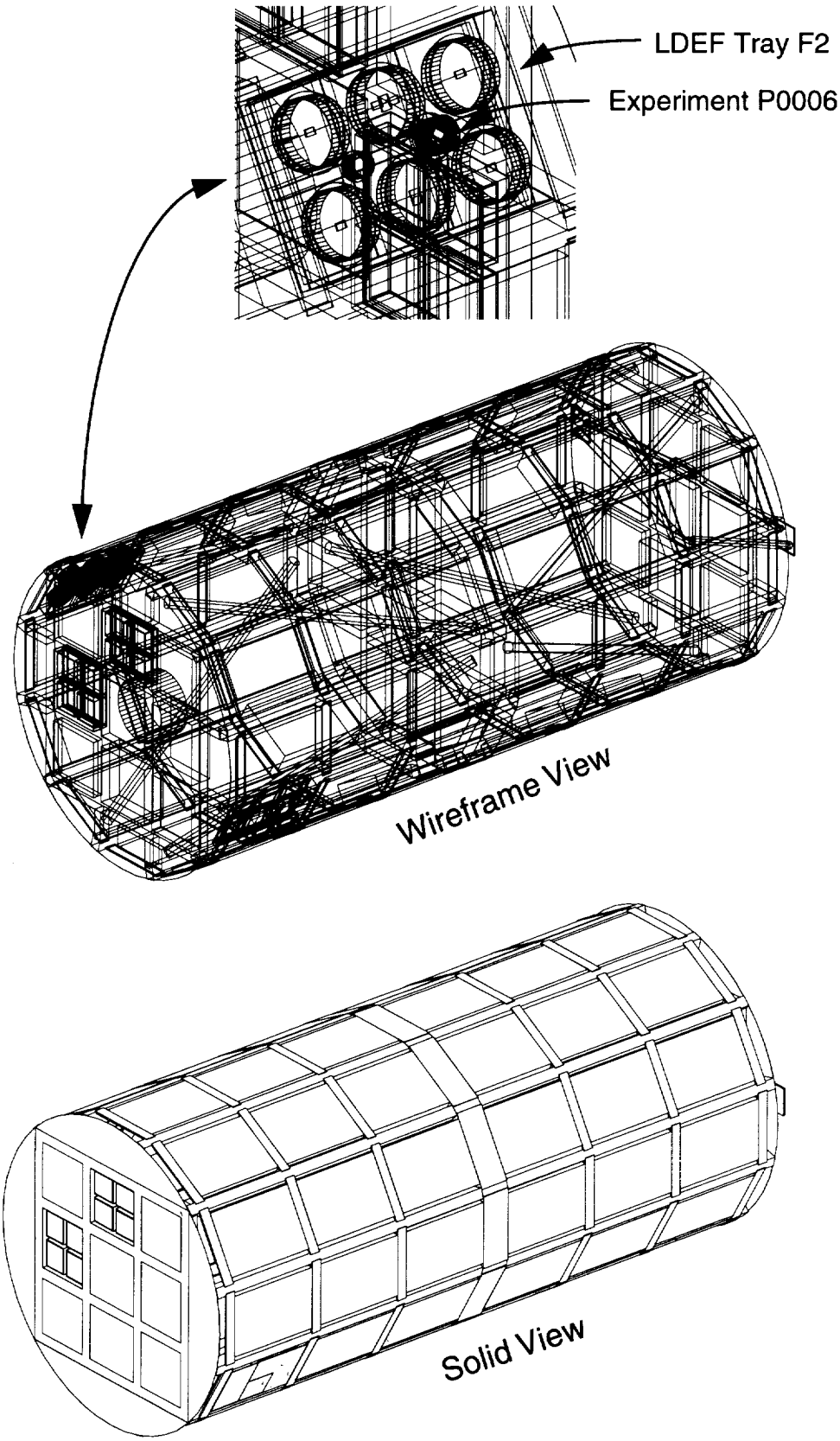

Fig. 1. CADrays version of LDEF satellite 3-D mass model with expanded view of Tray F2.

3. Trapped Proton Anisotropy

Measurements of the radioisotope ^{22}Na produced by proton bombardment in aluminum tray clamps at various locations around the LDEF spacecraft /32/, together with the fact that LDEF's orientation was very stable during the mission, provide data for checking the accuracy of current models for predicting the directionality of the trapped proton flux. Preliminary results of model/data comparisons for the tray clamp activation have been published previously /6,9,19/. Given here are results from recent calculations using two model/parameter revisions: a different trapped proton model and a different set of atmospheric scale heights. An overview of the calculational method is shown in Fig. 2.

Previous calculations were made using the standard AP8 trapped proton flux model /33/. Recently, Daly and Evans /34/ of the European Space Agency (ESA) have incorporated an improved interpolation method into the AP8 model. A comparison of the LDEF tray clamp activation using these two flux models is shown in Fig. 3. In both cases, the MSFC anisotropy model /35/ is used to predict the proton angular distribution. The ESA version of the AP8 model gives activation predictions that are about 30% higher than the standard AP8 model and in better agreement with the magnitude of the measured activation. Using the ratio of activation on the west (trailing) edge of LDEF to the east (leading) edge activation as a measure of the trapped proton anisotropy from Fig. 3, the measured anisotropy is about 1.6 compared to a predicted anisotropy of about 1.3. Averaged over all directions, the standard AP8 model predictions are 53% of the measured activation, and predictions using the ESA version of AP8 are 68% of the measured activation (Fig. 4).

To further investigate the sensitivity of the predictions to model/parameter assumptions, calculations for a different set of effective proton scale heights were made. Following Watts, et al. /35/, scale heights for initial calculations were based on atmospheric scale heights from the MSFC/J70 atmospheric model /36/ with "correction factors" from Heckman and Nakano /37/ then applied to get the effective (trajectory averaged) proton scale height. These proton scale heights, denoted as baseline values, are plotted in Fig. 5. As pointed out by Kern /38/, these estimated proton scale heights are substantially higher than some published values, such as those measured by Heckman and Brady /39/. Fits to the Heckman and Brady scale heights (denoted as revised values) are also shown in Fig. 5. The scale heights used at various times during the LDEF mission are given in Table 2.

Results using these revised scale heights, together with other calculational cases, are shown in Fig. 6 as curves A through F, and the corresponding model/parameter assumptions are summarized in Table 3. Curve A is from initial scoping calculations /19/ where the trapped proton

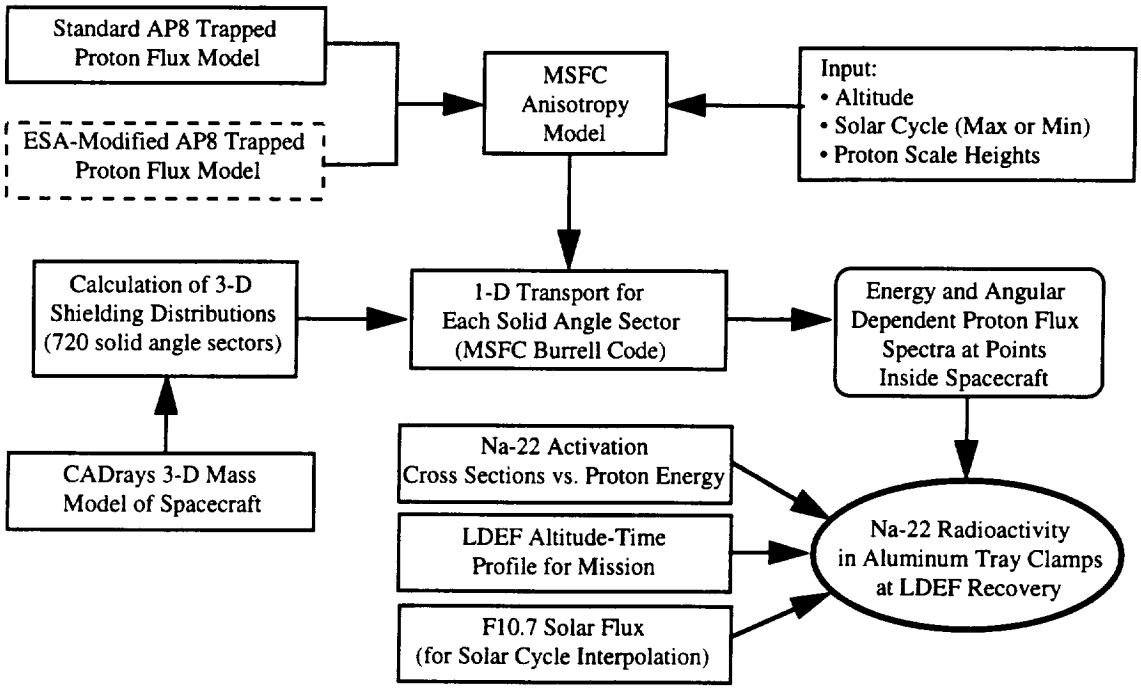

Fig. 2. Overview of calculational method used in predicting LDEF tray clamp activation.

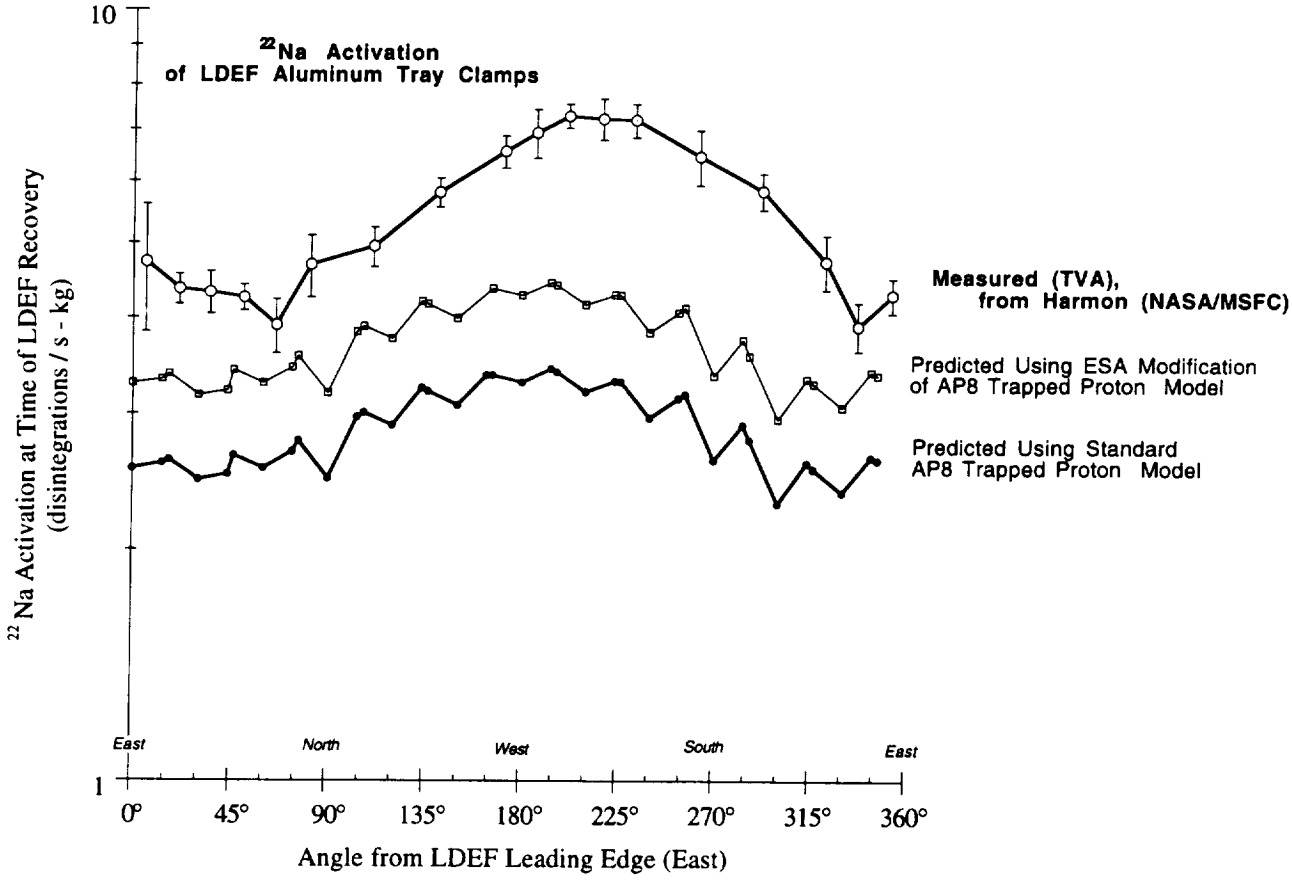

Fig. 3. Comparison of predicted and measured activation.

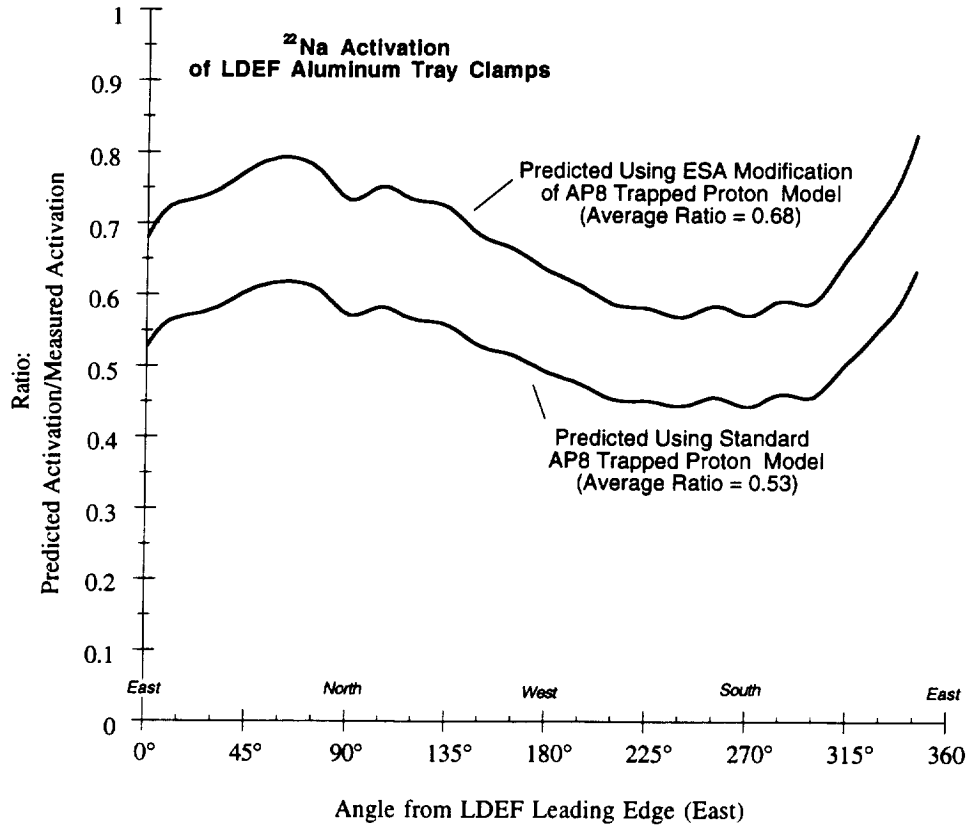

Fig. 4. Ratio of predicted to measured tray clamp activation as a function of direction.

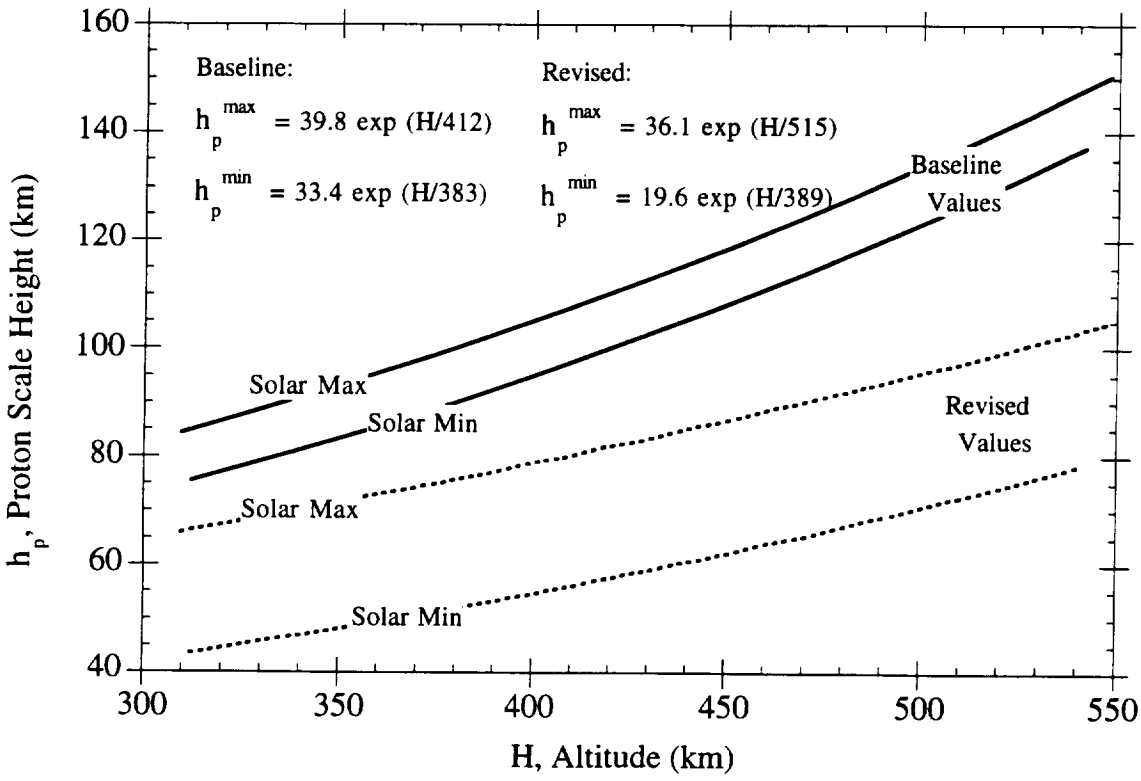

Fig. 5. Proton scale heights used as input for trapped proton anisotropy calculations.

Table 2. Scale heights used at different LDEF altitudes

Case	Mission Day	Altitude (km)	Flux Model	F10.7	Alpha	Proton Scale Height (km) "Baseline" (a)	Proton Scale Height (km) Revised (b)	Ratio: Revised/ Baseline
1A	0	478.7	AP8MIN	95	0.241	116.6	66.84	0.57
1B	0	478.7	AP8MAX	95	0.241	127.2	91.59	0.72
2	300	475.8	AP8MIN	67	0.000	115.7	66.35	0.57
3	1000	469.1	AP8MIN	67	0.000	113.7	65.21	0.57
4A	1300	466.2	AP8MIN	87	0.172	112.8	64.73	0.57
4B	1300	466.2	AP8MAX	87	0.172	123.4	89.40	0.72
5A	1500	461.5	AP8MIN	118	0.440	111.4	63.95	0.57
5B	1500	461.5	AP8MAX	118	0.440	122.0	88.58	0.73
6A	1700	449.5	AP8MIN	158	0.784	108.0	62.01	0.57
6B	1700	449.5	AP8MAX	158	0.784	118.5	86.54	0.73
7A	1800	433.6	AP8MIN	171	0.897	103.6	59.53	0.57
7B	1800	433.6	AP8MAX	171	0.897	114.0	83.91	0.74
8	1900	412.8	AP8MAX	183	1.000	108.4	80.59	0.74
9	2000	388.8	AP8MAX	183	1.000	102.3	76.91	0.75
10	2050	368.0	AP8MAX	183	1.000	97.2	73.87	0.76
11	2105	319.4	AP8MAX	183	1.000	86.4	67.21	0.78

(a) Based on MSFC/J70 atmospheric model /36/ for density scale heights with Heckman and Nakano /37/ corrections for effective proton scale height
(b) Based on Heckman and Brady /39/ proton scale heights

Table 3. Model and parameter assumptions for tray clamp activation calculations.

Calculational Case	Trapped Proton Model	Solar Cycle	Altitude	Scale Heights	Geometry Model	Comments
A	AP8	Solar Max	450 km	Baseline	Slab	Initial scoping calculations
B	AP8	LDEF Av.	LDEF Av.	Baseline	Detailed 3-D	Baseline case
C	AP8	LDEF Av.	LDEF Av.	Baseline	Hollow Cylinder	Check on 3-D geometry model
D	AP8	LDEF Av.	LDEF Av.	Baseline	Slab	} Flux incident from exterior only, to check contribution from "streaming"
E	AP8	LDEF Av.	LDEF Av.	Baseline	3-D	
F	AP8/ESA Mod	LDEF Av.	LDEF Av.	Baseline	3-D	Influence of trapped proton model
G	AP8/ESA Mod	LDEF Av.	LDEF Av.	Revised	3-D	Influence of scale height assumptions

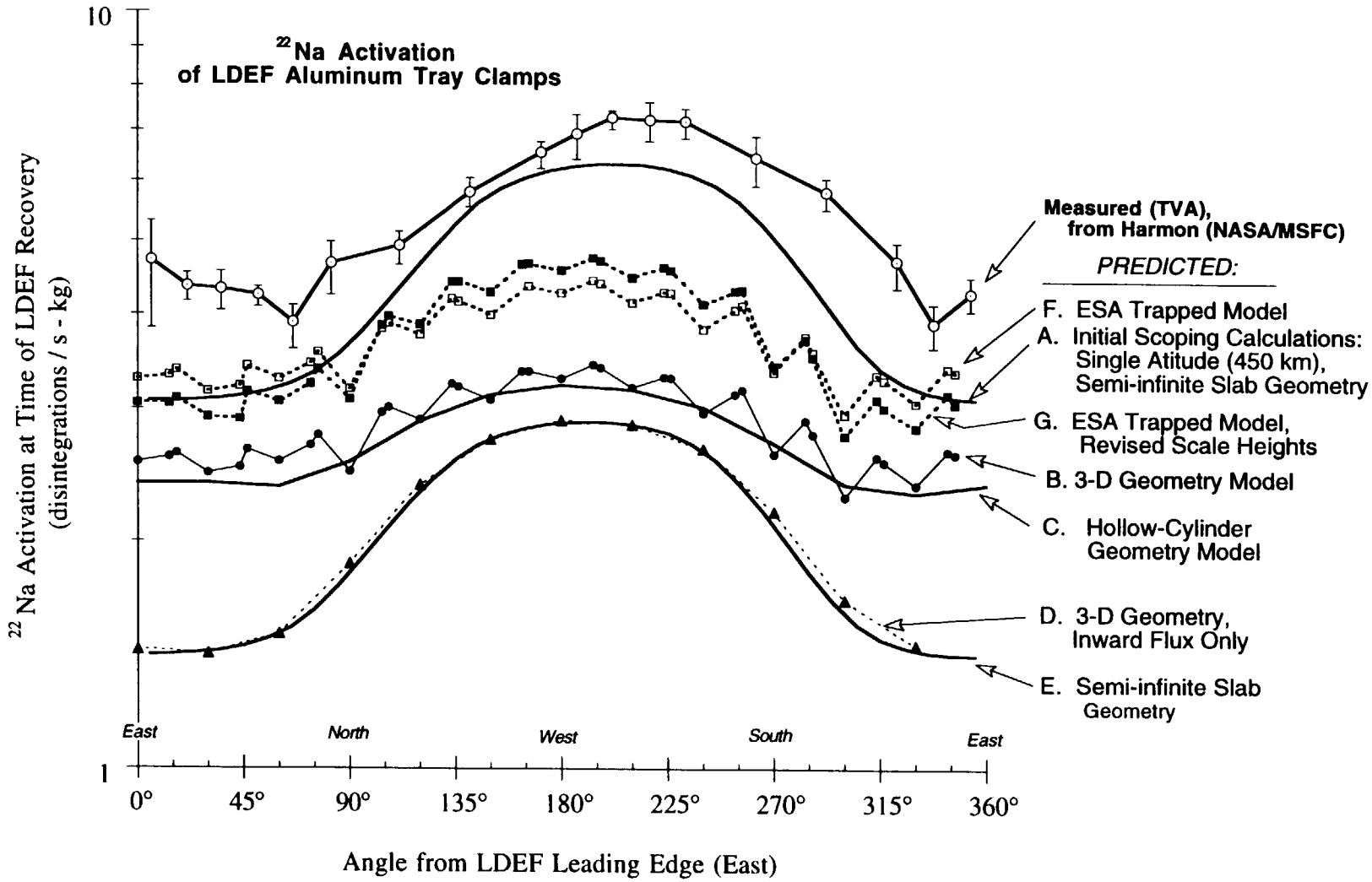

Fig. 6. Predictions of angular variation of LDEF tray clamp activation for different modeling assumptions.

environment (solar maximum) at a single altitude (450 km, corresponding approximately to the LDEF insertion altitude) was used and a semi-infinite slab geometry of aluminum was assumed for the LDEF spacecraft. For case B, the 3-D LDEF mass model and properly averaged trapped proton exposure (taking into account the LDEF altitude profile and interpolating between solar maximum and solar minimum using the F10.7 solar flux, as described in /18/) were used. This more accurate modeling procedure gives results that are considerably lower in magnitude and less directional than observed. As a check on the geometry model, a "hollow-cylinder" geometry was used (case C) in which all of the LDEF mass was placed (homogeneously) in a cylindrical geometry having an outer radius corresponding to the average outer radius of the spacecraft and an inner radius corresponding to the average depth of the experiment trays on LDEF. These results are in good agreement with the detailed geometry (case B), indicating that in the calculations there is a significant contribution to the tray clamp activation from protons streaming through the low-mass interior of the spacecraft and contributing to the activation while escaping the spacecraft in an outward direction. To check this, the activation was calculated for the 3-D geometry model considering only protons incident from directions exterior to the spacecraft (case D). As expected, case D shows more directionality, and is in good agreement with a calculation using a semi-infinite slab geometry (case E). (A comparison of the two semi-infinite slab cases, curves E and A, shows the effect of using the average exposure for the LDEF mission compared to the exposure at insertion.) Curve F is for the ESA version of AP8 and baseline scale heights (same curve as shown previously in Fig. 3), and curve G is for the ESA model and the revised set of scale heights listed in Table 2. The predicted activations using the revised scale heights are about 10% higher near west directions and about 10% lower near east directions compared to the baseline scale heights. The anisotropy in terms of west/east activation for predictions using the revised scale heights is 1.5, which can be compared with the ratios stated earlier of 1.3 for predictions using the baseline scale heights and 1.6 for the measurements. Therefore, the revised scale heights give results that are slightly more directional and in better agreement with the LDEF data.

In considering other modeling factors that influence the accuracy of the model/data comparisons, we note that the ^{22}Na activation cross section is relatively well-known, with an uncertainty less that about 15% based on the spread of measured data points in the energy range of interest here (see /27/). A contribution from secondary particles to the activation would be in the direction needed to obtain better model/data agreement. However, based on HETC transport code calculations that were made /7/, which took into account secondary protons and neutrons from trapped protons as well as the activation from galactic protons and secondary particles, these contributions were estimated to be less than $\approx$ 3% of the primary trapped proton activation calculated here.

The LDEF tray clamp data is well suited for checking anisotropy modeling since the measurements cover the complete angular range. However, a partial check of the tray clamp model/data comparisons can be made using LDEF absorbed dose data. Measurements of the radiation dose using thermoluminescent dosimeters (TLDs) were made on LDEF at locations near the trailing (west) and leading (east) sides of the spacecraft and for some cases at similar shielding depths, as summarized in /13, 17/. The predicted dose anisotropy, in terms of the ratio of trailing-to-leading edge TLD doses, is about 1.4 for the baseline scale heights compared to the measured ratio of about 2.4, as discussed in /13/. Thus, the predicted anisotropy is essentially the same for dose and tray clamp activation (1.4 vs. 1.3) whereas the measured anisotropy is somewhat higher for dose (2.4) than tray clamp activation (1.6).

4. Trapped Proton Flux

In addition to checking trapped proton directionality modeling as considered in the previous section, additional LDEF data (from the activation of metal samples, from fission foils, and dose measurements) can be utilized to evaluate model predictions of the angle-integrated trapped proton flux. Such model/data comparisons have been published previously (e.g., /13/) using the standard AP8 proton flux model, and example results for several different data sets at the same general location on LDEF (Experiment P0006, Tray F2) are shown in Fig. 7.

If the ESA version of the AP8 model is used for the trapped proton model, somewhat better agreement with measurements is obtained than published previously. An example comparison for the Exp. P0006 data is shown in Fig. 7. These results indicate that for the LDEF mission parameters the ESA version of the AP8 model underpredicts the flux by about 30% while the standard AP8 model underpredicts the flux by about 50%. Fig. 7 shows that the model/data ratio is approximately constant with shielding depth, indicating that is it the magnitude of the model fluxes that are in error, not the proton energy spectra.

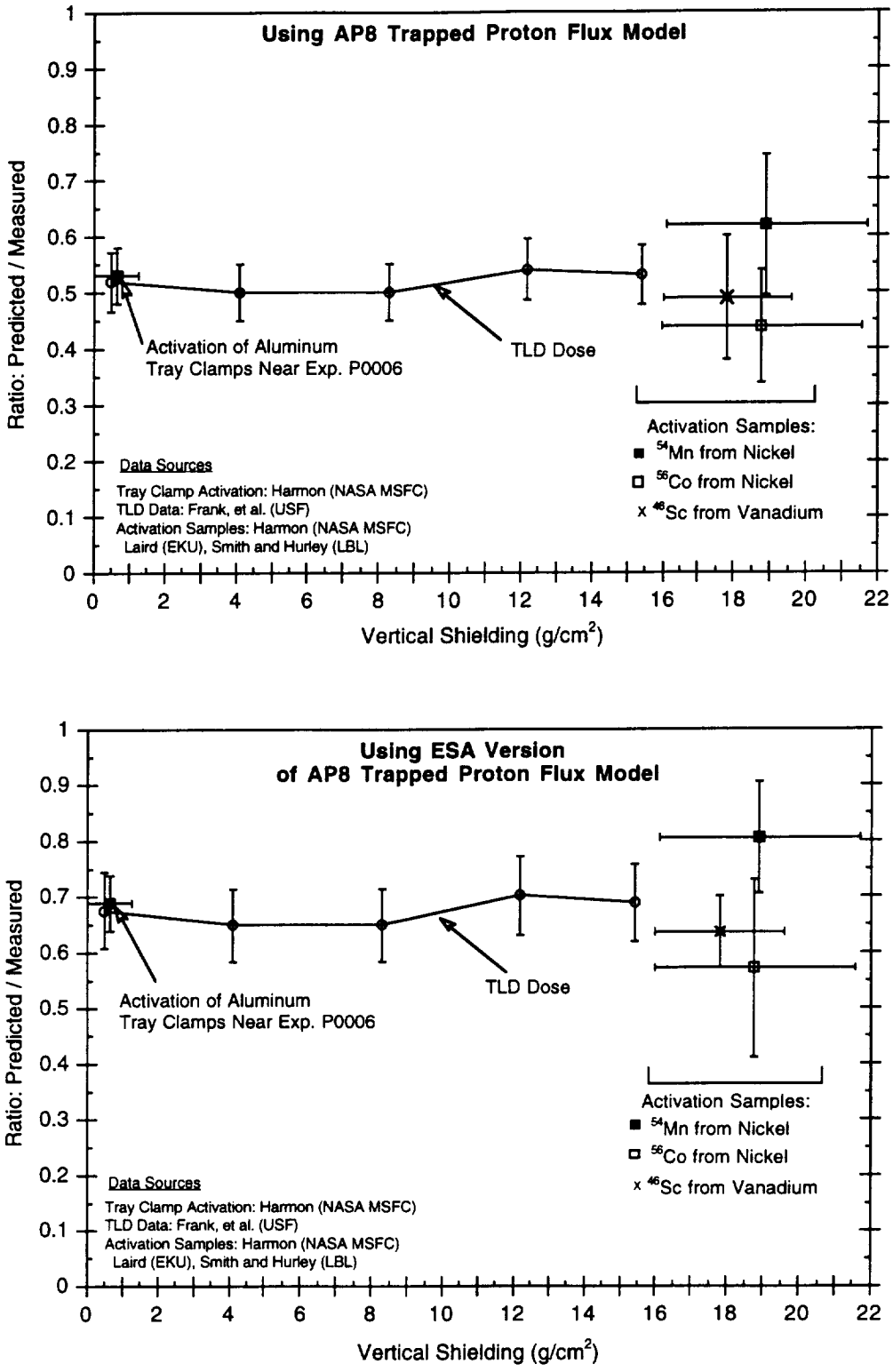

Fig. 7. Ratio of predicted to measured results for LDEF Experiment P0006 using standard AP8 trappped proton flux model (top) and ESA version of AP8 (bottom).

5. LET Spectra

5.1 Introduction

One of the more interesting results from the LDEF radiation dosimetry is the good statistical accuracy of the measured LET spectra, particularly at high LET (e.g., /40/), and the large difference between the observed spectra vs. pre-recovery LET predictions. Calculations to remove some of the simplifying assumptions made for the pre-recovery LET predictions /8/ are given in Appendix A. These calculations include: (a) taking into account shielding effects by using the 3-D mass model of LDEF, (b) a check on the contribution of projectile fragments - i.e., secondary particles from nuclear interactions by incident heavy ions in the cosmic ray spectrum, and (c) evaluation of the contribution from heavy ions due to solar flares during the mission.

With the above improvements to the LET prediction methods, the predicted spectra still differ significantly from measured spectra, as illustrated in Fig. 8. The divergence of the predicted and measured spectra at low LET is expected since the plastic detector (CR-39) is not able to detect short-range proton tracks and the low-LET part of the spectrum is dominated by trapped protons. (An integral of the predicted LET spectrum of Fig. 8, which is dominated by the trapped proton contribution at low LET, is in excellent agreement with the predicted absorbed dose from trapped protons at this position given in /13/.)

In considering the high-LET part of the spectrum, the geomagnetic cutoff for the LDEF orbit is $\approx 10^3$ MeV/nucleon (Fig. 9) so incident GCR ions (dominated by $Z \leq 26$) contribute mainly to the LET up to $\approx 10^3$ MeV/(g/cm^2), as indicated by the stopping power for Fe in Fig. 10, and this accounts for the sharp break in the predicted LET curve of Fig. 8. GCR Fe ions can contribute at higher LET as they slow down in thick portions of the spacecraft/payload shielding before reaching the detector, and this accounts for the predicted flux spectrum of Fig. 8 in the LET range from $\approx 2 \times 10^3$ to the maximum stopping power of 4×10^4 MeV/(g/cm^2) for Fe ions in CR-39.

Therefore, the flux of heavy ions in the GCR spectrum is too low to account for the flux in the highest LET portion of the observed spectrum. However, "target fragments" from trapped protons (not included in the predicted curve of Fig. 8) can contribute in this region, and calculations of this contribution are described below. These target fragments are the result of trapped proton nuclear interactions with C and O of the CR-39 (composition : $C_{12}H_{18}O_7$, density : 1.3 g/cm^3), and, from the stopping power curves of Fig. 10, can contribute at LET up to about 10^4 MeV/(g/cm^2).

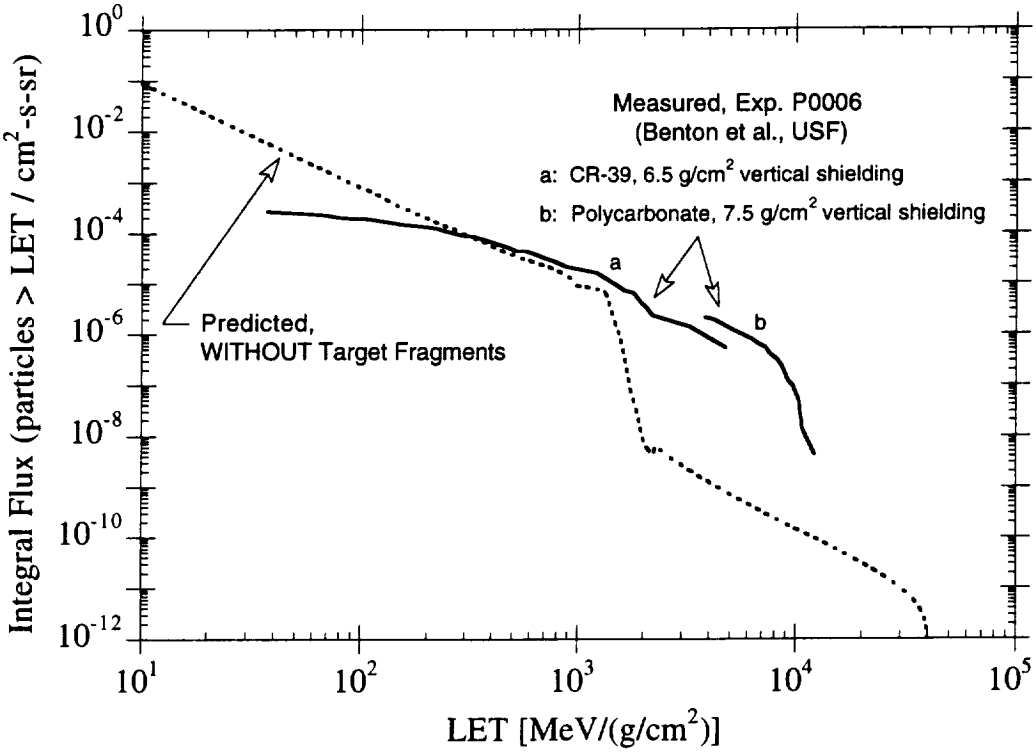

Fig. 8. LET spectra measured on LDEF compared to predictions. The predictions here neglect the contribution from recoil particles (target fragments) due to trapped proton nuclear interactions in the detector.

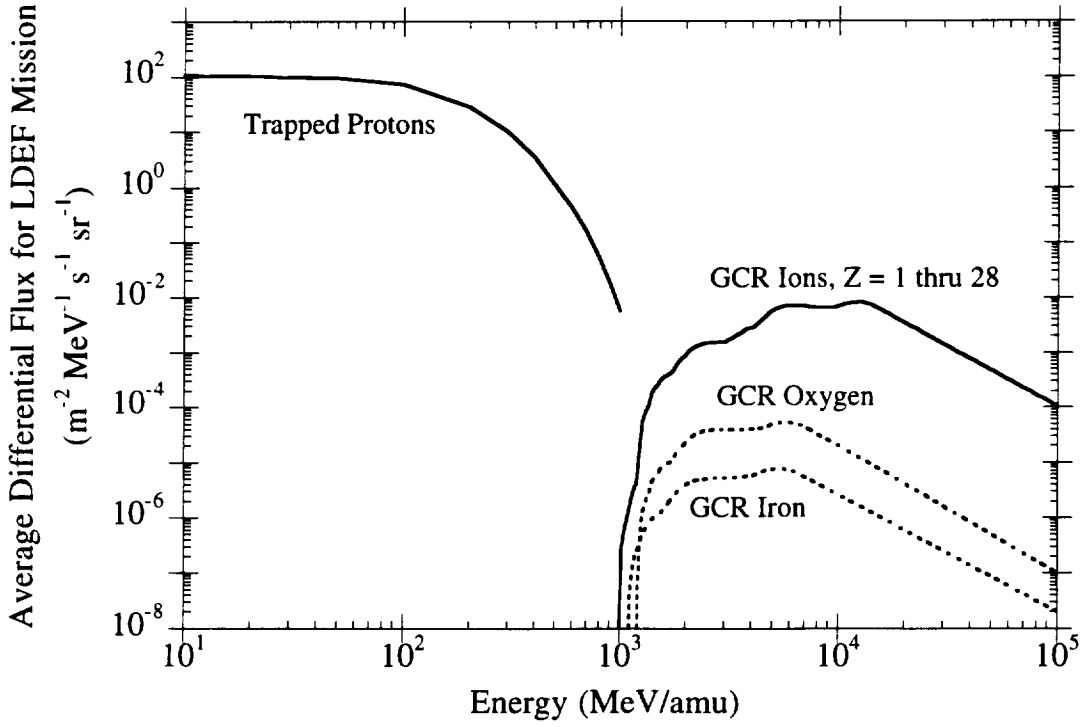

Fig. 9. Trapped proton and galactic cosmic ray spectra near LDEF surface (0.1 g/cm^2).

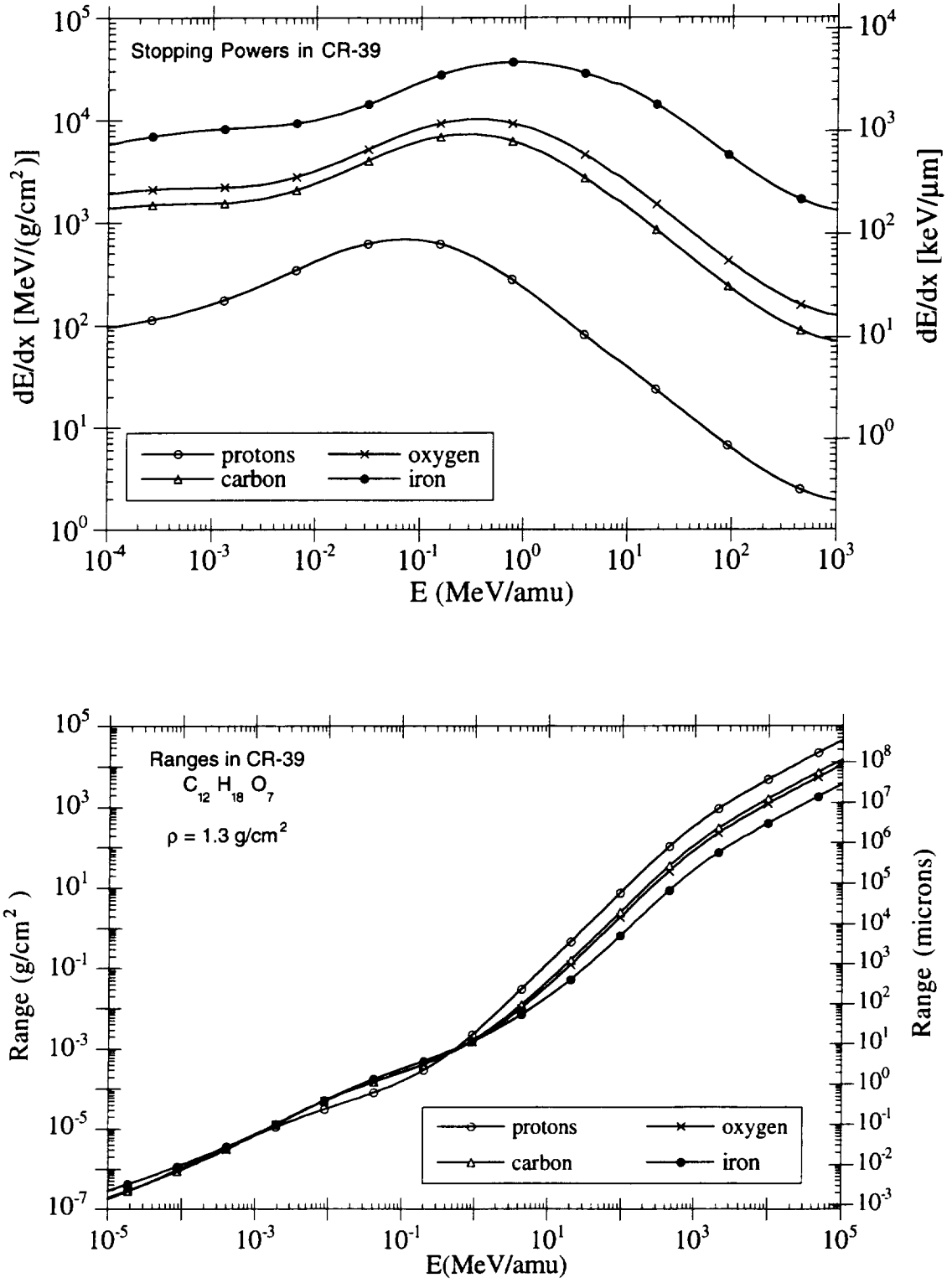

Fig. 10. Stopping powers and ranges in CR-39, calculated using SPAR code /4/.

5.2 Target Fragment Contribution to LET

The contribution of ion products from trapped proton nuclear interactions in the CR-39 detectors on LDEF has been calculated using the procedure outlined in Fig. 11. For the LDEF trapped proton exposure, the mission-average, angular-dependent ("vector") flux spectra (in 720 equal solid angle intervals) was determined using the AP8 flux model /33/, the MSFC anisotropy model /35/, and the altitude, mission time, and solar cycle averaging procedure described in /18/. The predictions here are at the position of a layer of thin (1mm) sheets of CR-39 located at a depth of 6.5 g/ cm^2 in the main detector stack of LDEF experiment P0006 in experiment tray F2. The LDEF mass model includes a detailed 3-D description of the P0006 detector and tray F2 components, as described in /29/ and indicated earlier in Fig. 1.

The trapped proton spectrum in the CR-39 (Fig. 12) was determined using the trapped proton environment and shielding model described above and transport calculations using the straightahead, continuous slowing down proton transport of Burrell /42/. The proton spectrum in the CR-39 was then used as a source for Monte Carlo transport calculations using the HETC code /43/. Nuclear collisions in the CR-39 (Fig. 13), and the energy and direction of each particle produced from collisions, are determined from a Monte Carlo calculation using the intranuclear-cascade-evaporation nuclear model in the HETC code. Results showing the contributions of various ions to the LET spectrum are shown in Fig. 14. It is assumed in the calculation that the CR-39 registers tracks with $dE/dx > 6$ keV/μm.

As described by Benton, et al. /40/, for the data analysis of the reported measurements at this location on LDEF a coincidence counting procedure was used where an ion track was counted only if it produces etch pits on adjacent surfaces of two CR-39 sheets. For the measurements of interest here, the etching procedure used removed a layer of about 8 μm from each CR-39 sheet. Therefore, to compare with these measurements, in the calculations a fixed reference boundary within the CR-39 was specified as the original (pre-etch) interface between two sheets. Then each ion from the Monte Carlo calculations was tested as to whether it crossed planes a distance G/2 μm on either side of the interface boundary, where G is the total "etch gap". Calculations were made for varying G values as a sensitivity check, with G = 16 μm corresponding to the etch gap for data analysis procedure used. Target fragment LET spectra for detection thresholds of G=0 (no etch gap, corresponding to actual LET spectrum expected) and G = 16 μm are shown in Fig. 15 together with the predicted GCR and trapped proton components for comparison. The sum of the predicted components are compared with the measured LET spectra in Fig. 16.

These calculations show that for the LDEF orbit there is a significant contribution at high LET in CR-39 detectors from target fragments. Furthermore, the target fragment contribution dominates the spectrum at LET beyond that where GCR ions above the geomagnetic cutoff for the

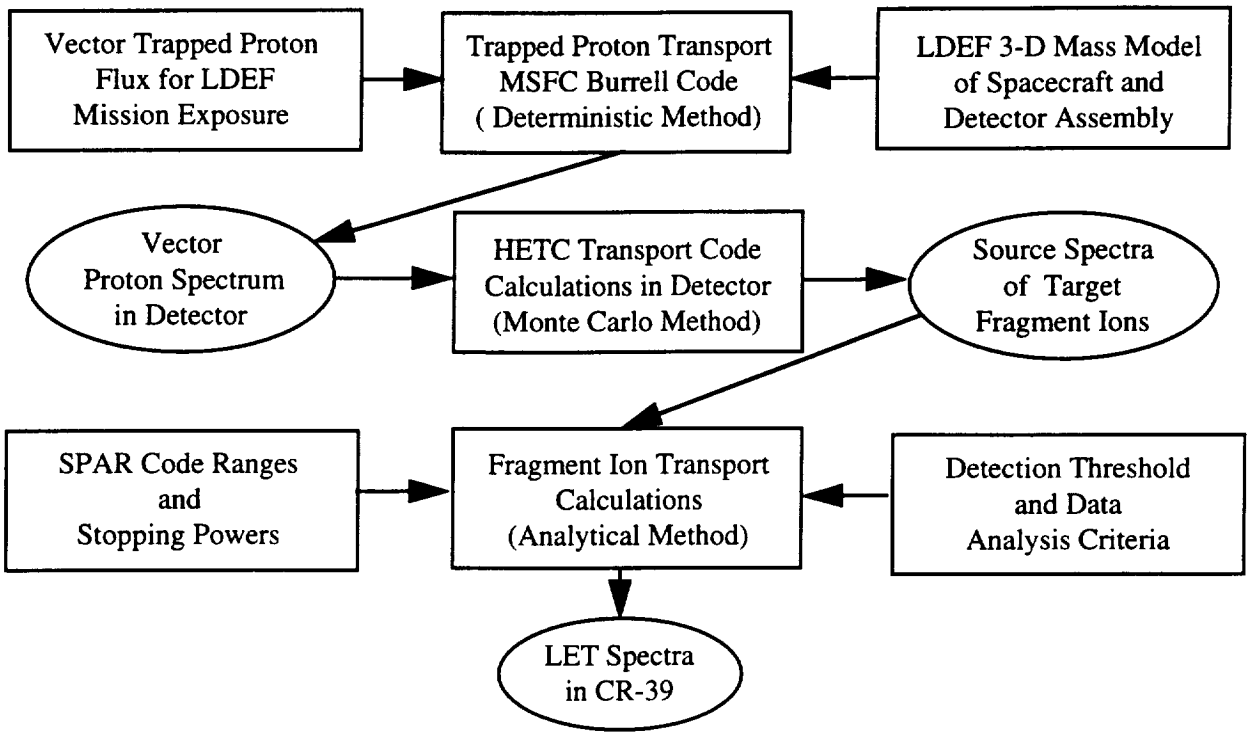

Fig. 11. Calculational method used for predicting contribution of target fragments to LET spectra in CR-39 plastic nuclear track detector on LDEF.

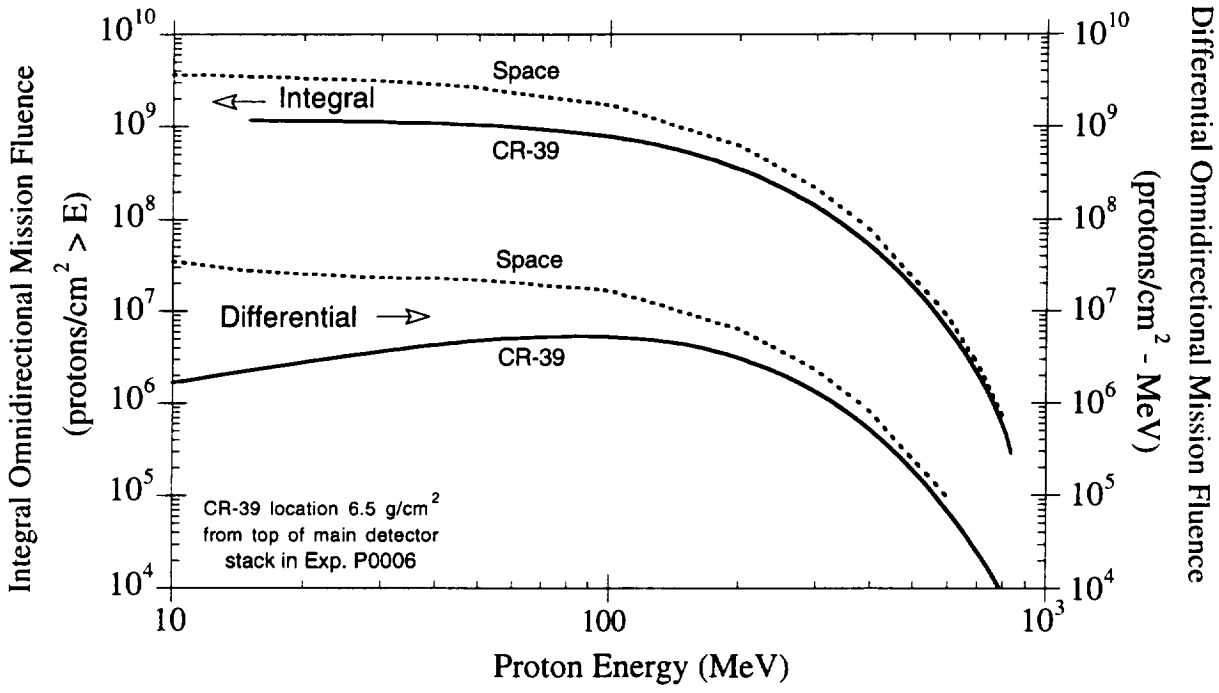

Fig. 12. Trapped proton fluence spectra (integrated over 720 equal solid angles of vector fluence) for LDEF mission. Curves labeled "space" are for ambient environment; curves labeled "CR-39" are in plastic nuclear track detector located 6.5 g/cm^2 from top of Exp. P006 detector stack.

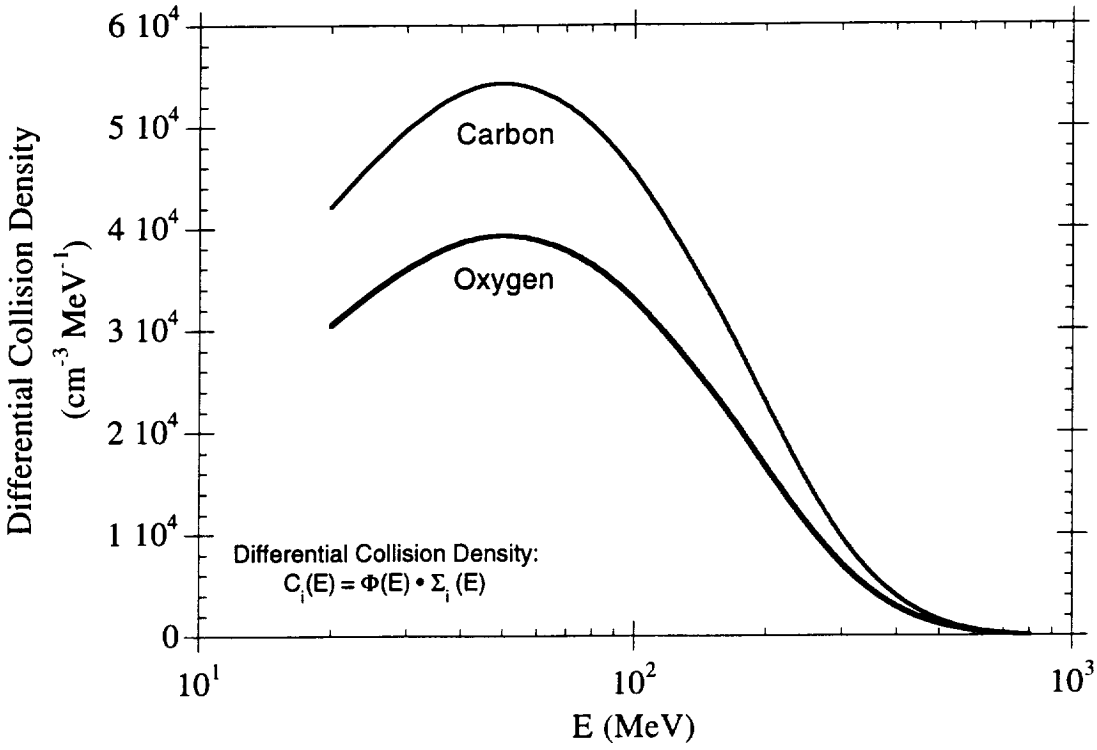

Fig. 13. Collision density from trapped proton nuclear interactions with carbon and oxygen in CR-39 of LDEF Exp. P006.

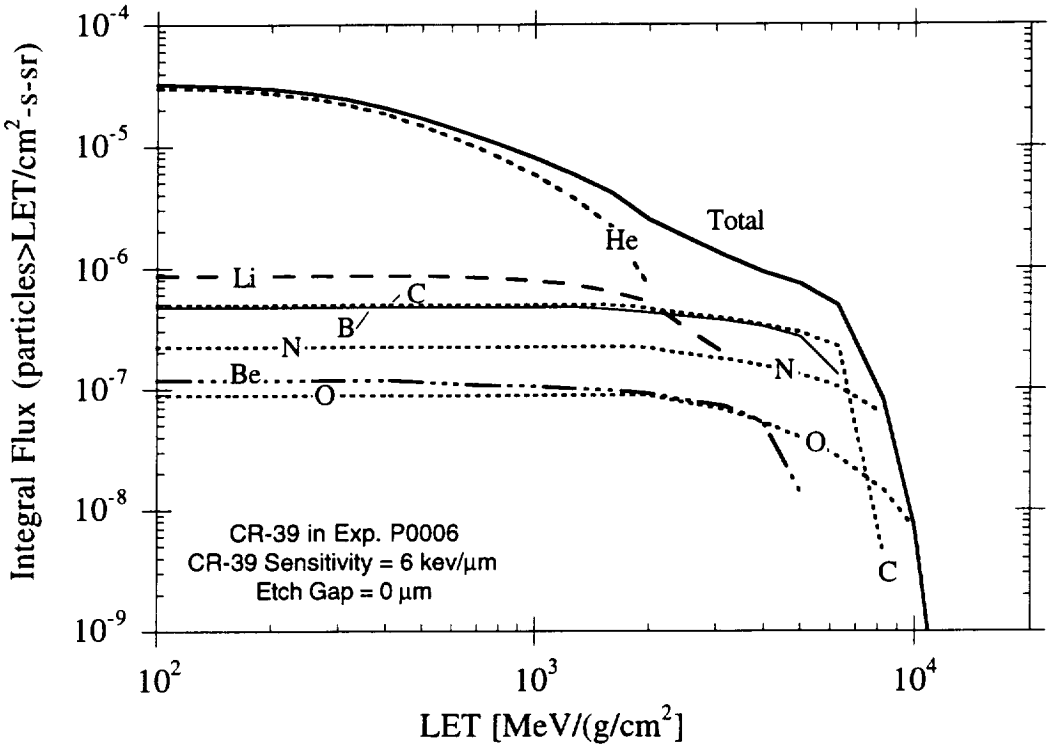

Fig. 14. HETC code prediction of ion contributions to LET from target fragments produced in CR-39 by trapped protons.

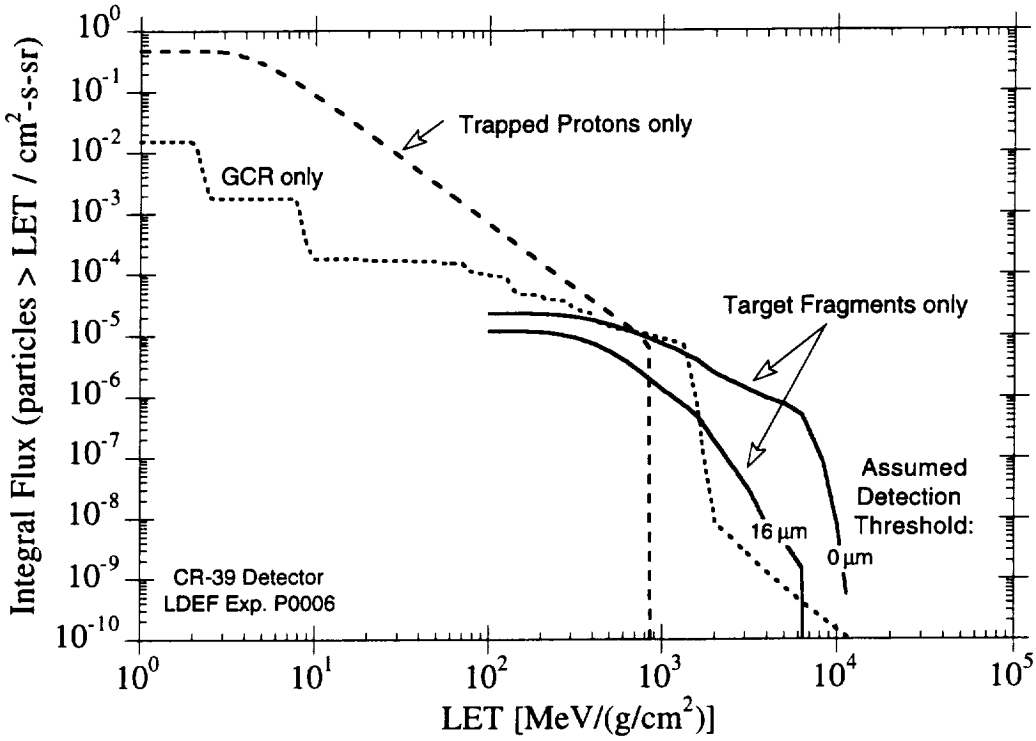

Fig. 15. Predicted components of LET spectrum in CR-39 plastic nuclear track detector in LDEF Experiment P0006.

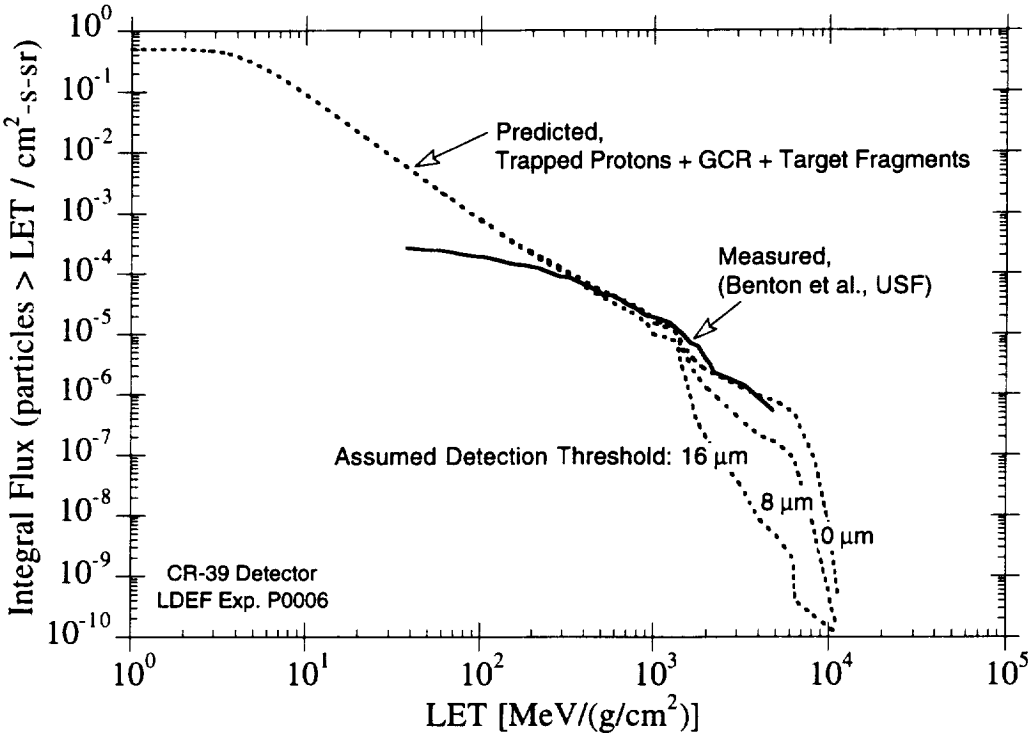

Fig. 16. Comparison of predicted and measured LET spectra.

LDEF orbit can contribute ($\approx 2 \times 10^3$ MeV·cm^2/g, Fig. 15). The calculations also indicate a strong dependence of the spectrum at high LET on the etching and data analysis methods employed, as evidence by the curves for different assumed etch gap thicknesses. Predictions for the etch gap thickness quoted for the measurements (16 μm) are much lower than the high-LET data (Fig. 16). The difference between calculated vs. measured LET spectra for target fragments is more than the factor of two underpredition attributed to the AP8 trapped proton model based on comparisons with the LDEF activation and absorbed dose data sets.

6. Bibliography of Publications Containing SAIC Contributions to LDEF Ionizing Radiation Analyses

Journal Papers

1. Armstrong, T. W.; Colborn, B. L.; and Watts, Jr., J. W.: Radiation Environment Model Uncertainties Based On LDEF Satellite Data. in preparation - to be submitted to *Nucl. Meas.*

2. Armstrong, T. W.; Colborn, B. L.; Harmon, B. A.; and Laird, C. E.: Prediction Of The Nuclear Activation of Materials on LDEF Produced by the Space Radiation Environment and Comparison with Flight Measurements. in preparation - to be submitted to *Nucl. Meas.*

3. Armstrong, T. W.; Colborn, B. L.; and Benton, E. V.: Model Calculations of the Radiation Dose and LET Spectra on LDEF and Comparison with Flight Data. in preparation - to be submitted to *Nucl. Meas.*

4. Colborn, B. L. and Armstrong, T. W. : Mass Model of the LDEF Satellite Spacecraft and Experiments for Ionizing Radiation Analyses. in preparation - to be submitted to Nucl. Meas.

5. Watts, Jr., J. W.; Armstrong, T. W.; and Colborn, B. L.: Predictions of LDEF Exposure to the Ionizing Radiation Environment. in preparation - to be submitted to *Nucl. Meas.*

6. Armstrong, T. W.; Colborn, B. L.; Harmon, B. A.; Parnell, T. A.; Watts, Jr., J. W. and Benton, E. V.: Comparison of Model Predictions with LDEF Satellite Radiation Measurements. *Adv. Space Res.* Vol. 14, No. 10, pp. 17-20, (1994).

7. Armstrong, T. W. and Colborn, B. L.: Predictions of Induced Radioactivity for Spacecraft in Low Earth Orbit. Nucl. Tracks Radiat. Meas., Vol. 20, No. 1, pp. 101-130, 1992.

8. Benton, E. V.; Heinrich, W.; Parnell, T. A.; Armstrong, T. W.; Derrickson, J. H.; Fishman, G. J.; Frank, A. L.; Watts, J. W., Jr. and Wiegel, B.: Ionizing Radiation Exposure of LDEF: Pre-recovery Estimates. *Nucl. Tracks. Radiat. Meas.* 20, 75 (1992).

Third LDEF Post-Retrieval Symposium Papers

9. Armstrong, T. W.; Colborn, B. L.; Harmon, B. A. and Laird, C. E.: Predictions of LDEF Radioactivity and Comparison with Measurements. Third LDEF Post-Retrieval Symposium, NASA CP-3275, 1993.

10. Armstrong, T. W.; Colborn, B. L. and Benton, E. V.: Predictions of LET Spectra Measured on LDEF. Third LDEF Post-Retrieval Symposium, NASA CP-3275, 1993.

11. Frank, A. L.; Benton, E. V.; Armstrong, T. W.; and Colborn, B. L.: Fission Foil Measurements of Neutron and Proton Fluences in the A0015 Experiment. Third LDEF Post-Retrieval Symposium, NASA CP-3275, 1993.

12. Watts, John W.; Armstrong, T. W.; and Colborn, B. L.: Status of LDEF Radiation Modeling. Third LDEF Post-Retrieval Symposium, NASA CP-3275, 1993.

Second LDEF Post-Retrieval Symposium Papers

13. Armstrong, T. W. and Colborn, B. L.: Radiation Model Predictions and Validation Using LDEF Satellite Data. Second LDEF Post-Retrieval Symposium, NASA CP-3194. 1992.

14. Armstrong, T. W. and Colborn, B. L.: Future Directions for LDEF Ionizing Radiation Modeling and Assessments. Second LDEF Post-Retrieval Symposium, NASA CP-3194. 1992.

15. Colborn, B. L. and Armstrong, T. W.: Development and Application of a 3-D Geometry/Mass Model for LDEF Satellite Ionizing Radiation Assessments. Second LDEF Post-Retrieval Symposium, NASA CP-3194. 1992.

16. Csige, I.; Benton, E. V.; Frigo, L.; Parnell, T. A.; Watts, Jr., J. W.; Armstrong, T. W. and Colborn, B. L.: Three-Dimensional Shielding Effects on Charged Particle Fluences Measured in the P0006 Experiment of LDEF. Second LDEF Post-Retrieval Symposium, NASA CP-3194. 1992.

17. Frank, A. L.; Benton, E. V.; Armstrong, T. W. and Colborn, B. L.: Absorbed Dose Measurements and Predictions on LDEF. Second LDEF Post-Retrieval Symposium, NASA CP-3194. 1992.

18. Watts, John W.; Armstrong T. W. and Colborn, B. L.: Revised Prediction of LDEF Exposure to Trapped Protons. Second LDEF Post-Retrieval Symposium, NASA CP-3194. 1992.

First LDEF Post-Retrieval Symposium Papers

19. Armstrong, T. W. and Colborn, B. L.: Ionizing Radiation Calculations and Comparisons with LDEF Data. First LDEF Post-Retrieval Symposium, NASA CP-3134. 1991.

20. Colborn, B. L. and Armstrong, T. W.: LDEF Geometry/Mass Model for Radiation Analyses. First LDEF Post-Retrieval Symposium, NASA CP-3134. 1991.

21. Watts, John W.; Parnell, T. A.; Derrickson, James H.; Armstrong, T. W. and Benton, E. V.: Prediction of LDEF Ionizing Radiation Environment. First LDEF Post-Retrieval Symposium, NASA CP-3134. 1991.

Conference Presentations

22. Armstrong, T. W.; Colborn, B. L.; and Watts, Jr., J. W.: Predictions of East-West Asymmetry Effects for Detailed Spacecraft Geometries. Presentation at Workshop on Radiation Belts: Models and Standards, Belgium Institute for Space Aeronomy, Bruessels, Belgium, 17-20 October, 1995 (to be published in workshop proceedings).

23. Armstrong, T. W.; Colborn, B. L.; Parnell, T. A.; Watts, Jr., J. W.; Harmon, B. A.; Benton, E. V. and Benton, E. R.: Evaluation of Space Radiation Modeling Uncertainties Using LDEF Satellite Measurements. Presentation at 32nd IEEE Nuclear and Space Radiation Effects Conference, Madison, WI, 17-21 July 1995.

24. Armstrong, T. W.; Colborn, B. L.; Harmon, B. A.; Parnell, T. A.; Watts, Jr., J. W.; and Benton, E. V.: Comparison of Model Predictions with LDEF Satellite Radiation Measurements. Presentation at the World Space Congress, Washington, D. C., 28 August - 5 September, 1992.

25. Armstrong, Tony W. and Parnell, Thomas A.: Opportunities for Addressing Ionizing Radiation Environment Issues Utilizing LDEF Satellite Data. Proceedings of the ESA Workshop on Space Environment Analysis, 9-12 October 1990, ESTEC, Noordwijk, The Netherlands, European Space Agency Report ESA WPP-23, 1990.

SAIC Reports

26. Armstrong, T. W. and Colborn, B. L.: LDEF Satellite Radiation Analyses. Science Applications International Corporation Report SAIC-TN-96035, March 1996. (This report)

27. Armstrong, T. W. and Colborn, B. L.: Proton Activation Cross Sections Used in Predicting LDEF Satellite Induced Radioactivity. Science Applications International Corporation Report SAIC-TN-96030, February 1996.

28. Armstrong, T. W. and Colborn, B. L.: LDEF Satellite Radiation Study. Science Applications International Corporation Report SAIC-94/8002, March 1994.

29. Colborn, B. L. and Armstrong, T. W.: Geometry and Mass Model of Ionizing Radiation Experiments on the LDEF Satellite. Science Applications International Corporation Report SAIC-TN-9202, April 1992.

30. Armstrong, T. W. and Colborn, B. L.: Scoping Estimates of the LDEF Satellite Induced Radioactivity. Science Applications International Corporation Report SAIC-90/1462, September 1990.

7. Other References

31. Colborn, B. L.; Ringler, S. J.;. Potter, D. W; and Armstrong, T. W.: CADrays 3-D Mass Model of International Space Station Alpha: Preliminary Version through Flight Assembly Stage 19A. Science Applications International Corporation Report SAIC-TN-9450, Nov. 1994.

32. Harmon, B. A.; Fishman, G. J.; Parnell, T. A; and Laird, C. E.: Induced Radioactivity in LDEF Components. First LDEF Post-Retrieval Symposium, NASA CP-3134, 1991.

33. Sawyer, D. M. and Vette, J. I.: AP-8 Trapped Proton Environment for Solar Maximum and Solar Minimum. National Science Data Center, Goddard Space Flight center, NSSDC/ WDC-A-R&S 76-06 (1976).

34. Daly, E. J. and Evans, H. D. R.: Problems in Radiation Environment Models at Low Altitudes. Memo ESA/ESTEC/WMA/93-067/ ED, April 1993.

35. Watts, J. W.; Parnell, T. A.; and Heckman, H. H.: Approximate Angular Distribution and Spectra for Geomagnetically Trapped Protons in Low Earth Orbit. AIP Conf. Proc., High Energy Radiation in Space (eds.: Rester, A. C., Jr. and Trombka, J. I.), Am. Inst. Phys., N.Y. (1989)

36. Johnson, D. L. and Smith, R. E.: The MSFC/J70 Orbital Atmosphere Model and the Data Bases for the MSFC Solar Activity Prediction Technique. NASA-TM-86522 (1965).

37. Heckman, H. H. and Nakano, G. H.: Low-Altitude Trapped Protons During Solar Minimum Period, 1962-1966. J. Geophys. Res., 74, 3575 (1969).

38. Kern, John W.: A Note on Vector Flux Models for Radiation Dose Calculations. Rad. Meas. 23, no. 1, 43 (1994).

39. Heckman, H. H. and Brady, V. O.: Effective Atmospheric Losses for 125-MeV Protons in South Atlantic Anomaly. J. Geophys. Res., 71, 2791 (1966).

40. Benton, E. V.; Csige, I.; Oda, K.; Henke, R. P.; Frank, A. L.; Benton, E. R; Frigo, L. A.; Parnell, T. A.; Watts, Jr, J. W; and Derrickson, J. H.: LET Spectra Measurements of Charged Particles in the P0006 Experiment on LDEF. Second LDEF Post-Retrieval Symposium, NASA CP-3194, 1992.

41. Armstrong, T. W. and Chandler, K. C.: Stopping Powers and Ranges for Muons, Charged Pions, Protons, and Heavy Ions. Nucl. Instr. Meth. 113, 313 (1973).

42. Burrell, M. O.: The Calculation of Proton Penetration and Dose Rates. NASA Marshall Space Flt. Ctr. Report NASA TM X-53063, August 1964.

43. Armstrong, T. W. and Colborn, B. L.: A Thick-Target Radiation Transport Code for Low-Mass Heavy Ion Beams, HETC/LHI. Nucl. Instr. Meth. 169 (1980).

Appendix A

Predictions of LDEF Radioactivity and Comparisons with Measurements

Paper presented at Third LDEF Post-Retrieval Symposium
Published in NASA CP-3275 (1993)

PREDICTIONS OF LDEF RADIOACTIVITY AND COMPARISON WITH MEASUREMENTS*

T. W. Armstrong and B. L. Colborn
Science Applications International Corporation**
Route 2, Prospect, TN 38477
Phone: 615/468-2603, Fax: 615/468-2676

B. A. Harmon
NASA Marshall Space Flight Center
Huntsville, AL 35812
Phone: 205/544-4924, Fax: 205/544-7754

C. E. Laird
Department of Physics, Eastern Kentucky University**
Richmond, KY 40475
Phone: 606/622-1526, Fax: 606/622-1020

ABSTRACT

As part of the program to utilize LDEF data for evaluation and improvement of current ionizing radiation environment models and related predictive methods for future LEO missions, calculations have been carried out to compare with the induced radioactivity measured in metal samples placed on LDEF. The predicted activation is about a factor of two lower than observed, which is attributed to deficiencies in the AP8 trapped proton model. It is shown that this finding based on activation sample data is consistent with comparisons made with other LDEF activation and dose data. Plans for confirming these results utilizing additional LDEF data sets, and plans for model modifications to improve the agreement with LDEF data, are discussed.

INTRODUCTION

The measured activation of materials on LDEF from radioactivity induced by trapped proton and cosmic ray environments provides an important data set for checking

*Submitted for publication in Proceedings of Third LDEF Post-Retrieval Symposium; Williamsburg, Virginia, 8-12 Nov. 1993.
**Work supported by NASA Marshall Space Flight Center, Huntsville, Alabama.

the accuracy of environment models and associated calculational methods for predicting the activation of spacecraft and payload materials in low-Earth orbit. Such modeling accuracy is of particular interest in radiation background assessments and component material selection in the design of space-based sensors.

In the present work, predictions have been made to compare with the observed radioactivity in several metal samples intentionally placed on LDEF as activation experiments. Model comparisons with LDEF activation measurements of spacecraft components and with thermoluminscent dosimetry (TLD) data have been reported previously (refs. 1,2). A result from these previous model/data comparisons is an estimate of the accuracy of the current AP8 trapped proton model for low-Earth orbit applications. The activation experiment sample data considered here provide an important additional data set for model comparisons by allowing a consistency check of the different data sets, previous model/data comparisons, and previous conclusions related to quantifying the trapped proton environment modeling uncertainties.

The activation experiment samples consisted of the metals nickel, tantalum, vanadium, indium, and cobalt placed in experiment trays at various locations on LDEF (Table 1), with sample sizes typically 2 in. x 2 in. and either 0.125 or 0.25 in. thick (ref. 3). A total of some 20 radioisotopes have been measured from these samples. We have not made predictions to compare with all of the measured radioisotopes for the following reasons: First, the primary objective of the present calculations is to compare with those radioisotopes which are produced by primary trapped protons so that previous conclusions on the accuracy of the AP8 model derived from model comparisons with other LDEF data can be checked. Some estimates are included here for isotopes produced by secondary neutrons and galactic cosmic rays, but the calculational method used for these estimates is less rigorous than than that used for the trapped proton produced isotopes. Secondly, the activation cross sections needed in predicting certain isotopes are not adequately known to provide the prediction accuracy needed in evaluating trapped proton model uncertainties. For these reasons, the predicted isotopes here are restricted to the nickel and vanadium samples.

The model comparisons made here with activation sample data provide a measure of the trapped proton flux model uncertainties, but information on the trapped proton anisotropy is difficult to interpret from these data because the samples are under different amounts of shielding at different locations (Table 2). The tray clamp activation data, which provide a detailed spatial mapping and are mostly free of shielding effects, provide a better data set for anisotropy model evaluations, as addressed in ref. 2.

The activation modeling approach has been to perform detailed calculations so that differences between the predicted and measured activations can be attributed to uncertainties in the incident radiation environment. Thus, as described below, predictions are based on a detailed treatment of the trapped proton environment (taking into account proton anisotropy, flux altitude dependence with mission time, and solar cycle dependence) and radiation transport using a detailed 3-D mass model of the LDEF spacecraft and experiment trays to account for shielding effects.

PREDICTION METHODS

Radiation Environment -- The LDEF trapped proton exposure predicted by Watts, et al. (ref. 4) is used, which is based on: the AP8 omnidirectional flux model (ref. 5), the anisotropy model of Watts, et al. (ref. 6) to obtain directionality of the incident flux spectrum, a detailed altitude dependence during the LDEF mission, and an interpolation of the solar minimum (AP8MIN) and solar maximum (AP8MAX) versions of the AP8 model according to the F10.7 cm. solar flux to account for solar cycle variations of the proton flux during the mission. For incident galactic protons, the LDEF orbit-average exposure from ref. 7 was used, which is based on the interplanetary spectrum of Adams (ref. 8).

Shielding Model -- The 3-D mass model developed for LDEF radiation analyses (ref. 9) was used. This model was extended for the present calculations to incorporate each of the activation samples -- i.e., the actual size and location of all of the individual activation samples were included in the shielding model.

Radiation Transport -- For incident trapped protons, radiation transport calculations were made using the Burrell primary proton transport code (ref. 10) and the 3-D mass model of LDEF with the activation samples included. At each spatial point in the activation samples where flux spectra were calculated, an angular grid of 720 equal solid angle bins around the point was defined, with a different energy spectrum incident in each solid angle to account for the trapped proton directionality. For examining activation produced by incident galactic protons, particle spectra (primary protons, secondary neutrons and protons) from previous (ref. 7) Monte Carlo (HETC code) transport calculations for a simple geometry model (1-D slab of aluminum) were used. Thus, the activation estimates from the galactic environment is approximate due to the geometry simplification, but, as discussed above, the trapped proton activation is the main interest here.

Radioisotope Production -- Flux spectra calculated at the center of each activation sample were folded with measured activation cross sections (shown later) compiled from the literature to compute radioisotope production as a function of time during the mission,

with decay rates then applied to obtain the radioactivity at LDEF recovery. (As a check on the approximation of using the flux only at the center of the sample, volume-average fluxes from a fine grid of flux points were computed for several samples and compared with the single point flux; the resulting activations agreed to within about 10% or less).

PREDICTED VS. MEASURED SAMPLE ACTIVATION

A summary of the LDEF activation sample measurement results is given in Table 3. Final data analyses and intercomparisons of measurements at different facilities have not yet been completed for all of the isotopes produced (ref. 11), so the data shown here are preliminary at present.

Vanadium Activation

Activation data for the vanadium sample are well suited for model comparisons because: vanadium has a single target isotope (99.75% ^{51}V) and a single measured radioisotope (^{46}Sc), so the production mode is well defined for predictions; the activation cross section is well known (Fig. 1); and the energy threshold for ^{46}Sc production is relatively low ($\approx$ 30 MeV), so the production is almost all ($\approx$ 96%) from incident primary trapped protons rather than from secondaries or galactic cosmic rays.

A comparison of the measured and calculated ^{46}Sc activation for the vanadium samples is shown in Fig. 2. Both the measured and calculated activities indicate only a small dependence on sample locations, suggesting that differences that might be expected due to the trapped proton anisotropy are masked by differences in shielding (Table 2). The average ratio of predicted to measured activity for samples at all locations is 0.49 ± 0.11.

Nickel Activation

Predictions for the nickel sample activation are not as simple as for vanadium because there are various production modes (Table 4), requiring a large number of activation cross sections (e.g., Fig. 3 for proton induced reactions), and secondary neutrons are important in producing some of the isotopes. A comparison of predicted vs. measured activities for the nickel sample in Exp. P0006 (Fig. 4) shows that trapped protons dominate the production of ^{54}Mn and ^{56}Co, but neutrons dominate the ^{58}Co and ^{60}Co production, and cosmic rays dominate the ^{46}Sc production due to its high energy threshold. The calculated and measured activities for nickel samples at all locations are compared in Table 5. The

average ratio of predicted-to-measured activities for the two isotopes (^{54}Mn and ^{56}Co) produced by primary trapped protons for all samples is 0.56 ± ≈ 0.08.

Solar Minimum vs. Solar Maximum Activation

Since LDEF exposure to trapped protons during the early part of the mission was at solar minimum and during the latter part at solar maximum (Fig. 5), activities for long vs. short half-life isotopes can be used to investigate uncertainty differences in the solar minimum (AP8MIN) vs. solar maximum (AP8MAX) trapped proton models. For example, Fig. 6 shows the case of a relatively short half-life product (^{46}Sc from V sample in Exp. P0006, 84 day half-life). Two curves are shown: the production rate vs. mission time, and the contribution of the production at times during the mission to the activity at recovery, which shows that the recovery activity for this isotope is due to proton exposure during solar maximum. The predicted-to-measured activity ratio in this case is 0.49 ± 0.11. For a long half-life isotope where the activity is at recovery due exposure during solar minimum, we use the ^{54}Mn activity (half-life = 303 days) for the same nickel sample in Exp. P0006, for which the predicted/measured ratio is 0.60 ± 0.12. Therefore, from comparisons with LDEF activation data we find no major difference in the AP8MIN vs. AP8MAX model uncertainties.

MODEL COMPARISONS WITH OTHER LDEF RADIATION DATA

The above comparisons of predicted vs. measured activities for the activation samples placed on LDEF indicate that the AP8 model underpredicts the trapped proton flux for the LDEF mission by about a factor of two. This result is consistent with model comparisons with other LDEF data, as summarized below.

Figure 7 compares predicted and measured ^{22}Na production in the aluminum clamps holding the experiment trays on LDEF, which has been published previously (ref. 2). The average predicted/measured activation around the spacecraft is 0.55 ± about 0.15 (Fig. 7). This ratio is in agreement with dose predictions that have been compared (ref.1) with TLD doses measured on LDEF (ref. 12) at shielding depths where the dose is due to trapped protons.

Figure 8 summarizes predicted vs. measured results for three different sets of data (tray clamp activity, TLD dose, and radioisotopes in activation samples) at the same location on LDEF (Exp. P0006 in Tray F2). These results show that the model/data

comparisons are consistent for the different data sets and that the predictions are about a factor of two lower than all of the data sets.

Another data set suitable for including in the comparisons of Fig. 8 is the fission tracks measured from fission foils (^{181}Ta, ^{209}Bi, ^{232}Th, and ^{238}U) included in Exp. P0006 (ref. 13). While these foils respond to protons and neutrons from both trapped and galactic proton sources, an estimate based on particle spectra from 1-D Monte Carlo calculations (ref. 7) shows that the energy dependence of the fission cross section for the Bi foil is such that fission tracks are produced predominately by trapped protons. Detailed calculations taking into account 3-D shielding effects have not yet been made to compare with these data.

Preliminary comparisons of predicted vs. measured activation of the steel trunnions on LDEF, which indicate somewhat better agreement than determined here for the activation samples, have been reported (ref. 14). However, this early work was of a scoping nature and several approximations were made in the predictions (e.g., the current estimate, ref. 4, of the trapped proton environment for LDEF was not available at that time), so these early trunnion activation calculations need to be revised before definitive trunnion data comparisons can be obtained.

SUMMARY

The predictions made here for the activation of metal samples placed on LDEF confirm results from previous comparisons with spacecraft component (tray clamp) activation data and TLD dosimetry data that radiation effects measured on LDEF that are due to the trapped proton environment are underpredicted by about a factor of two. These results indicate that the AP8 trapped proton model underpredicts the actual environment by a factor of two. Additional calculations to compare with other data sets (trunnion activation and fission foil measurements) are planned to further check this conclusion.

An investigation of model improvements that would give better agreement with the LDEF data is also planned. For example, predicted vs. measured differences for the trapped proton anisotropy is likely due to the approximate nature of the effective atmospheric scale heights currently used as input to the anisotropy model, and work to determine more accurate effective scale height estimates is planned. Also, recent work at the European Space Agency (ESA), ref. 15, shows that improvement to some of the numerical interpolation procedures used in the AP8 model increases the predicted trapped proton flux for low-Earth orbits, and comparisons with LDEF data using the ESA version of the AP8 model are planned.

REFERENCES

1. Armstrong, T. W. and Colborn, B. L.: Radiation Model Predictions and Validation Using LDEF Satellite Data. Second LDEF Post-Retrieval Symposium, NASA CP-3194, 1993.

2. Armstrong, T. W.; Colborn, B. L.; Harmon, B. A.; Parnell, T. A.; Watts, J. W. and Benton, E. V.: Comparison of Model Predictions with LDEF Satellite Radiation Measurements. *Adv. Space Res.* 14, No. 10, 17 (1994).

3. Harmon, B. A.; Fishman, G. F.; Parnell, T. A.; Benton, E. V. and Frank, A. L.: LDEF Radiation Measurements: Preliminary Results. *Nucl. Tracks Radiat. Meas.* 20, 131 (1992).

4. Watts, J. W.; Armstrong, T. W. and Colborn, B. L.: Revised Predictions of LDEF Exposure to Trapped Protons. Second LDEF Post-Retrieval Symposium, NASA CP-3194, 1993.

5. Sawyer, Donald W. and Vette, James I.: AP8 Trapped Proton Environment for Solar Maximum and Solar Minimum. National Science Data Center, Goddard Space Flight Center, NSSDC/WDC-A-R&S 76-06, Dec. 1976.

6. Watts, J. W., Jr.; Parnell, T. A. and Heckman, H. H.: Approximate Angular Distribution and Spectra for Geomagnetically Trapped Protons in Low-Earth Orbit, in: *High Energy Radiation Background in Space,* Proc. AIP Conf.., Vol. 186, pp. 75-85, American Institute of Physics, New York, 1989.

7. Armstrong, T. W. and Colborn, B. L.: Predictions of Induced Radioactivity for Spacecraft in Low-Earth Orbit. *Nucl. Tracks Radiat. Meas.* 20, 101 (1992).

8. Adams, James H., Jr.: Cosmic Ray Effects on Microelectronics. Part IV. NRL Memorandum Report 5901, December 1986.

9. Colborn, B. L. and Armstrong, T. W.: Development and Application of a 3-D Geometry/Mass Model for LDEF Satellite Ionizing Radiation Assessments. Second LDEF Post-Retrieval Symposium, NASA CP-3194, 1993.

10. Burrell, M. O.: The Calculation of Proton Penetration and Dose Rates. George C. Marshall Space Flight Center, Huntsville, AL., NASA TM X-53063, August 1964.

11. Harmon, Alan B.; Parnell, Thomas A. and Laird, Christopher E.: Status of LDEF Activation Measurements and Archive. (These Proceedings).

12. Frank, A. L.; Benton, E. V.; Armstrong, T. W. and Colborn, B. L.: Absorbed Dose Measurements and Predictions on LDEF. Second LDEF Post-Retrieval Symposium, NASA CP-3194, 1993.

13. Benton, E. V.: LDEF Experiment P0006 Linear Energy Transfer Spectra Measurement (LETSME). Evil Research, Inc. Final Report to NASA Marshall Space Flight Center, December 1990.

REFERENCES (CONTD)

14. Armstrong, T. W.; Colborn, B. L. and Watts, J. W.: Ionizing Radiation Calculations and Comparisons with LDEF Data. First LDEF Post-Retrieval Symposium, NASA CP-3134, 1991.

15. Daly, E. J. and Evans, H. D. R.: Problems in Radiation Environment Models at Low Altitudes. European Space Agency/ESTEC, preprint.

16. Smith, Alan R. and Hurley, Donna L.: Radioactivities of Long Duration Exposure Facility (LDEF) Materials: Baggage and Bonanzas. First LDEF Post-Retrieval Symposium, NASA CP-3134, 1991.

17. Winn, Willard G.: Gamma-ray Spectrometry of LDEF Samples at SRL. First LDEF Post-Retrieval Symposium, NASA CP-3134, 1991.

18. Laird, Christopher E.: Eastern Kentucky Univ., pri. comm.

19. Harmon, B. A.; Fishman, G. J.; Parnell, T. A. and Laird, C. E.: Induced Activation Study of LDEF. Second LDEF Post-Retrieval Symposium, NASA CP-3194, 1993.

20. Reeves. James H.: Arthur, Richard J. and Brodzinski, Ronald L.: Sensitivity of LDEF Foil Analyses Using Ultra-Low Background Germanium vs. Large NaI (Tl) Multidimensional Spectrometers. Second LDEF Post Retrieval Symposium, NASA CP-3194.

21. Harmon, B. Alan: NASA Marshall Space Flight Center, pri. comm.

Table 1. Location of activation samples on LDEF.

Contained in Exp. No.	Exp. Tray	Tray Position	Activation Samples				
P0006	F2	Trailing Side		Ni	V	Ta	In
A0114	C9	Leading Side	Co			Ta	In
A0114	C3	Trailing Side		Ni	V		
M0001	H12	Space End	Co	Ni	V	Ta	In
M0002	G12	Earth End	Co	Ni	V	Ta	In

Table 2. Vertical shielding for activation samples.

	Vertical shielding (g/cm^2) of activation sample in LDEF experiment tray:				
Sample	H-12	G-12	C-3	C-9	F-2
V	thermal cover	2.8	1.7		13
Ni	thermal cover	2.8	1.7		13
Co	thermal cover			1.7	13
Ta	thermal cover	8.0		1.7	13
In	thermal cover	8.0		1.7	13

Table 3. Summary of LDEF activation sample measurements - preliminary.

		Tray H12 (space end) Exp. M0001		Tray G12 (Earth end) Exp. M0002		Tray C9 (leading side) Exp. A0114		Tray C3 (trailing side) Exp. A0114		Tray F2 (trailing side) Exp. P0006	
Activation Sample	Product Isotope	Activity (pCi/kg)	Ref.	Activity (pCi/kg)	Ref.	Activity (pCi/kg)	Ref.	Activity (pCi/kg)	Ref.	Activity (pCi/kg)	Ref.
Nickel	Sc-46							11 ± 4	(c)	1.6 ± 0.4	(a)
	Mn-54	52 ± 7.8 72 ± 3.6	(c) (d)	25 ± 3.4 39 ± 8	(e) (c)			68 ± 6	(c)	27 ± 0.9	(a)
	Co-56	66 ± 28 70 ± 2.6	(c) (d)	29 ± 4.8 62 ± 27	(e) (c)			61 ± 9	(c)	33 ± 1.3 67 ± 16	(a) (c)
	Co-57	400 ± 7.2 395 ± 15	(c) (d)	403 ± 35 399 ± 23	(e) (c)			466 ± 18	(c)	322 ± 2 360 ± 24	(a) (c)
	Co-58	73 ± 3.4	(d)	62 ± 7.3 93 ± 17	(e) (c)			59 ± 11	(c)	42 ± 1.6 69 ± 11	(a) (c)
	Co-60	7.6 ± 3.4 9.0 ± 0.87 12 ± 7.8	(d) (g) (c)					11 ± 4	(c)	4.7 ± 0.3	(a)
Tantalum	Lu-172	56 ± 2.1	(h)	40 ± 1	(h)			75 ± 2	(h)	47 ± 1 36 ± 1.1	(h) (a)
	Lu-173	120 ± 9.8	(h)	171 ± 12	(h)			143 ± 5	(h)	91 ± 4 161 ± 8.3	(h) (a)
	Hf-175	38 ± 5.7	(h)	19 ± 2	(h)			39 ± 2	(h)	25 ± 2 37 ± 1.9	(h) (a)
	Ta-182	116 ± 8.1	(h)	45 ± 4	(h)			38 ± 2	(h)	135 ± 4 90 ± 2.3	(h) (a)
Vanadium	Sc-46	21 ± 6.0 13 ± 1.7	(b) (g)	16 ± 1.3 16 ± 1.4	(b) (e)	20 ± 1.5 24 ± 2.0 19.5 ± 11	(b) (h) (c)			17 ± 1.1 21 ± 2.7	(a) (c)
Indium	Rh-102	2.2 ± 0.6	(a)	2.3 ± 0.3	(a)	3.2 ± 0.4	(a)			2.2 ± 0.9	(a)
	Ag-110m	3.2 ± 0.8	(a)	2.3 ± 0.3	(a)	3.9 ± 0.5	(a)			5.1 ± 1.0	(a)
	Sn-113	35 ± 4.2	(a)	21 ± 1.2 22 ± 3.8	(a) (e)	41 ± 2.7 47 ± 19	(a) (c)			54 ± 3.6	(a)
	In-114m	190 ± 115	(a)	35 ± 15	(a)	55 ± 35	(a)			105 ± 20	(a)
Cobalt	Mn-54			91 ± 3.8 62 ± 1.4	(e) (f)	41 ± 1.1	(a)				
	Co-56			22 ± 3.8	(e)						
	Co-57			303 ± 5.4 211 ± 1.6	(e) (f)	125 ± 1.6	(a)				
	Co-58			116 ± 20	(e)						
	Co-60	204 ± 20	(g)	26 ± 2.2 23 ± 0.8	(e) (f)	19 ± 0.5 27 ± 2.7	(a) (g)				

(a) LBL measurements (Smith and Hurley, ref. 16)
(b) SRL measurements (Winn, ref. 17)
(c) MSFC/EKU measurements (Laird, ref. 18))
(d) Battelle measurements (from Laird, ref. 18)
(e) LLNL measurements (Camp, from Harmon, ref. 19)
(f) LBL measurements (Smith and Hurley, from Harmon, ref. 19)
(g) Battelle measurements (Reaves, ref. 20)
(h) JSC measurements (D. Lindstrom, ref. 21)

Table 4. Production modes for nickel activation products.

Product	Half-life	Production by Protons	Production by Neutrons	Production by Decay
Sc-46	83.8 days	Ni-58 (p,8p5n) Sc-46 Ni-60 (p,8p7n) Sc-46		
Mn-54	303 days	Ni-58 (p,4p1n) Mn-54 Ni-60 (p,4p3n) Mn-54		
Co-56	77 days	Ni-58 (p,2p1n) Co-56 Ni-60 (p,2p3n) Co-56		Ni-58(p,p2n)Ni-56 $\xrightarrow[6.1\ d]{EC}$ Co-56
Co-57	270 days	Ni-58 (p,2p) Co-57 Ni-60 (p,2p2n) Co-57	Ni-58 (n,np) Co-57	Ni-58(p,pn)Ni-57 $\xrightarrow[36\ hr]{EC,\beta+}$ Co-57
Co-58	71.3 days	Ni-60 (p,2pn) Co-58	Ni-58 (n,p) Co-58	Co-58m $\xrightarrow{9.2\ hr}$ Co-58g
Co-60	5.26 years	Ni-62 (p,2pn) Co-60	Ni-60 (n,p) Co-60	Co-60m $\xrightarrow{10.5m}$ Co-60g

Table 5. Ratio of predicted-to-measured activity at recovery for nickel activation samples.

	Sample Location on LDEF			
Isotope	Exp. P0006	Exp. A0114	Exp. M0002	Exp. M0001
Sc-46	0.29			
Mn-54	0.62	0.34	0.58	0.38
Co-56	0.44	0.69	0.78	0.64
Co-57	0.46	0.48	0.46	0.63
Co-58	0.53	0.70	0.44	0.57
Co-60	0.84	0.50		
AVERAGE:	0.53	0.54	0.57	0.55
Average for all isotopes in all samples: 0.55 ± ≈ 0.1				

Data Sources: Harmon (NASA MSFC) Smith and Hurley (LBL) Reeves (PNWL)
Laird (EKU) Camp (LLNL)

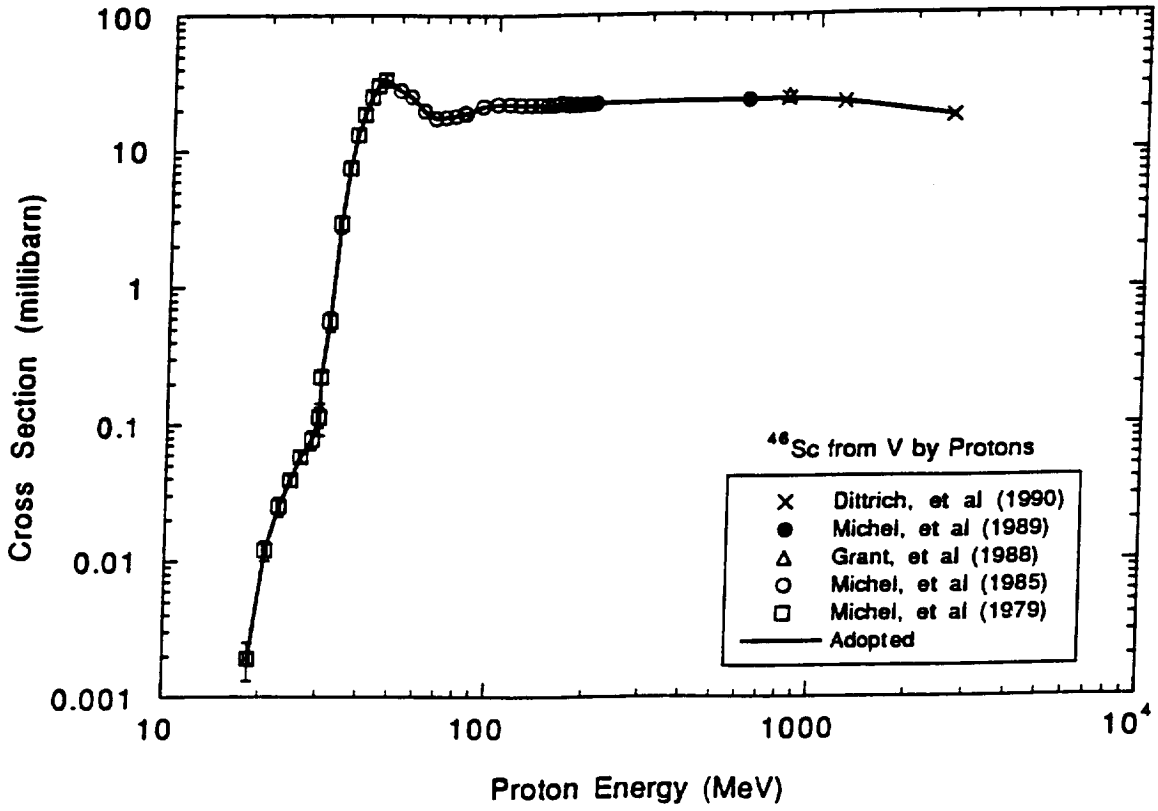

Fig. 1. Cross section for the production of ^{46}Sc from vanadium by protons; points represent measured cross sections.

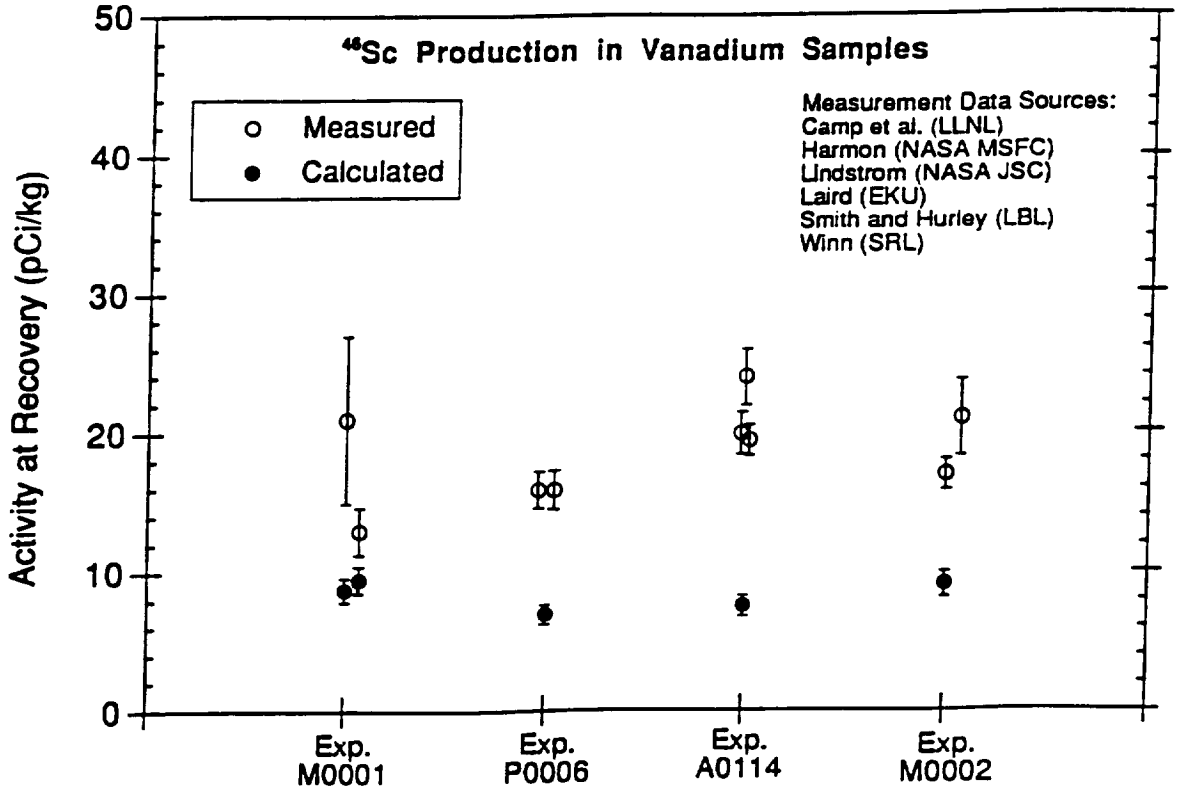

Fig. 2. Comparison of calculated and measured ^{46}Sc activation from vanadium samples.

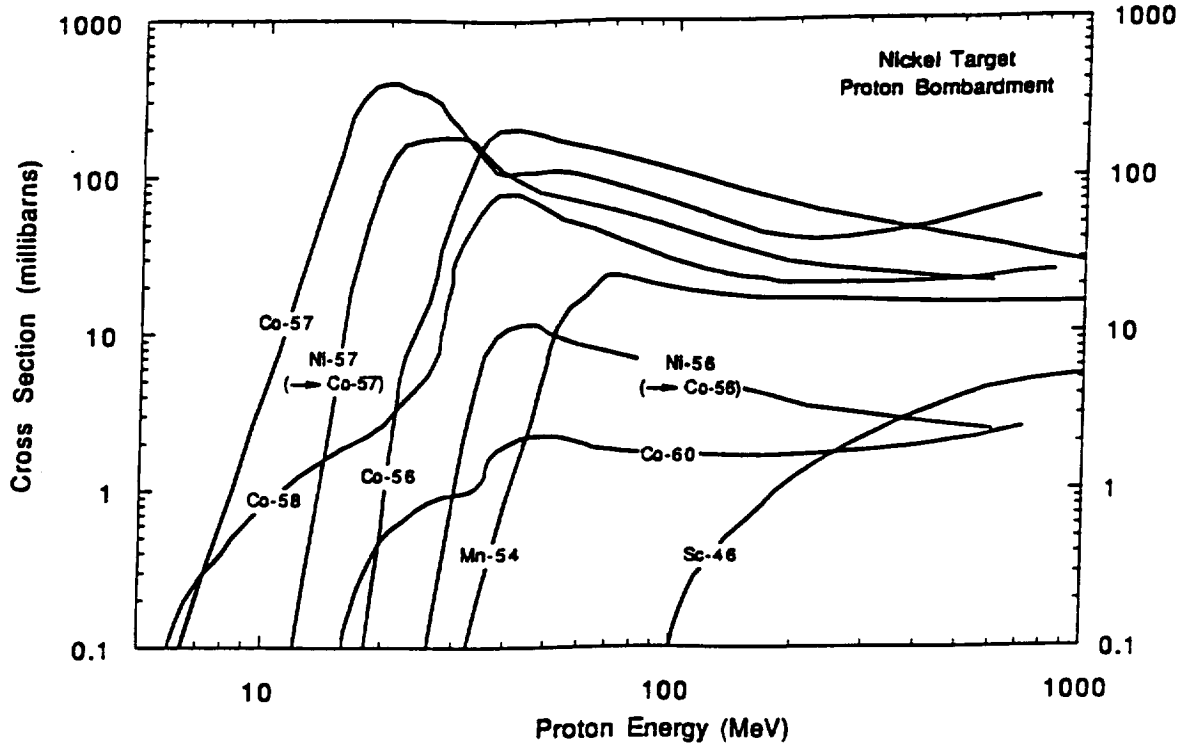

Fig. 3. Cross sections for the production of radioisotopes in nickel by protons, based on measured cross sections compiled from various sources.

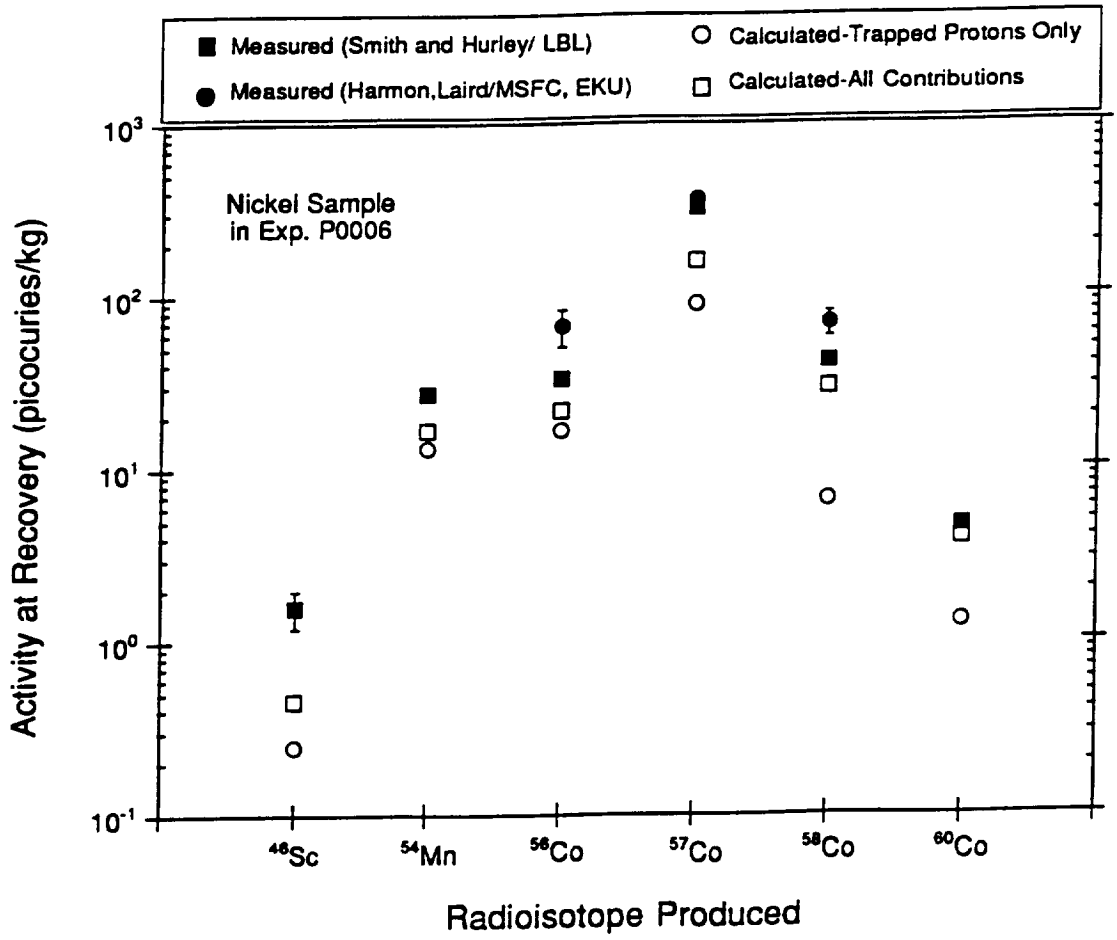

Figure 4. Comparison of predicted vs. measured (preliminary) activation products from nickel sample contained in LDEF Exp. P0006.

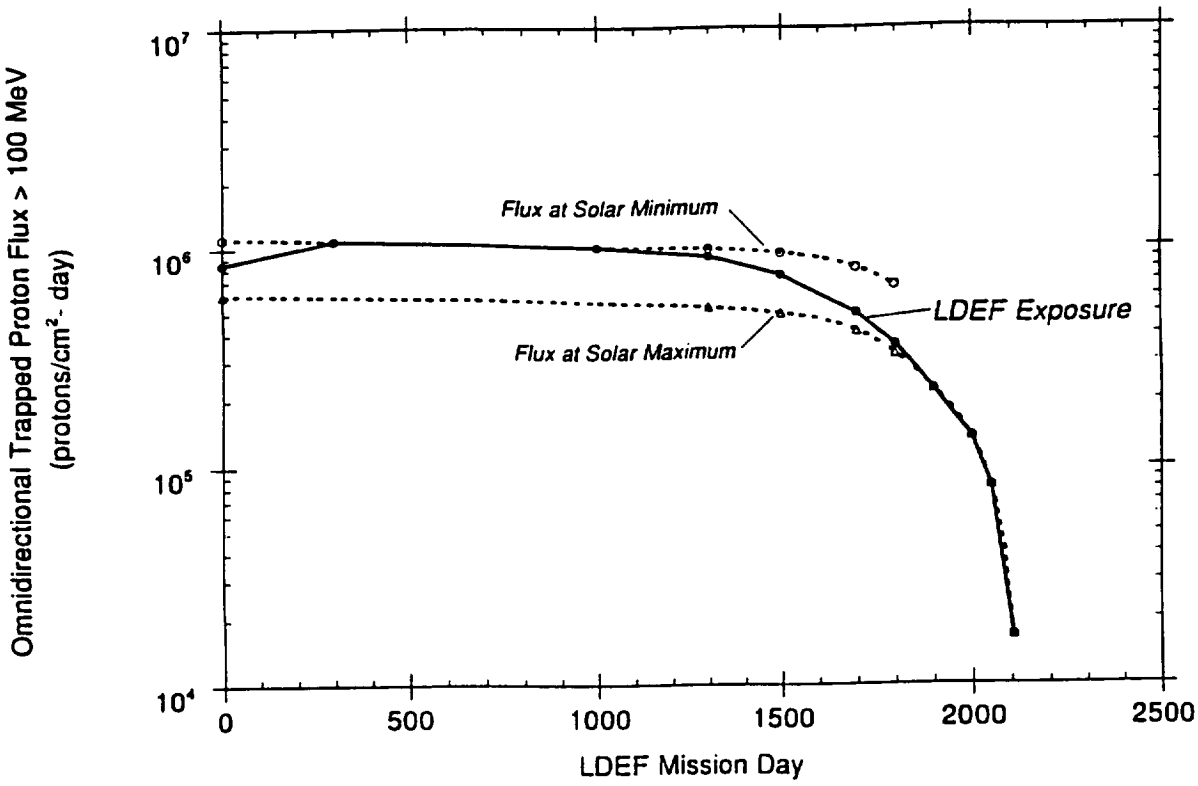

Fig. 5. Predicted trapped proton flux > 100 MeV during LDEF mission, from ref. 4.

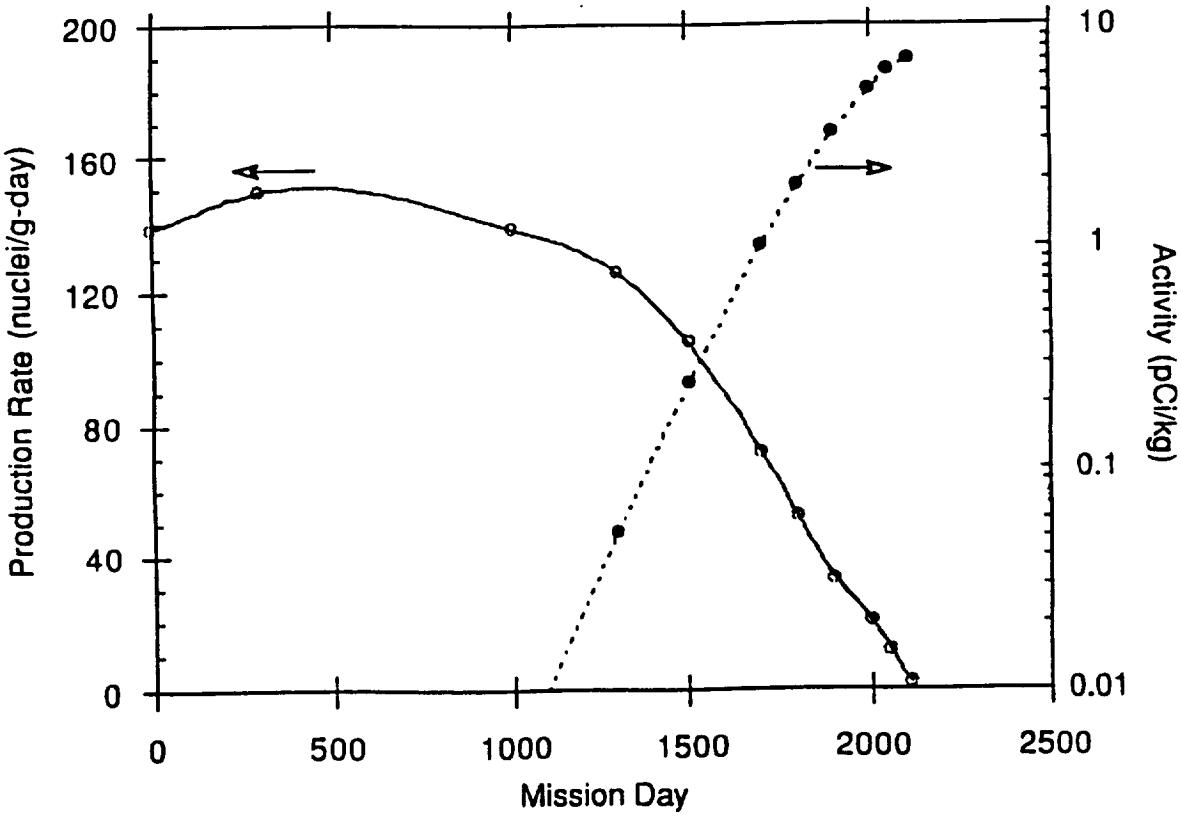

Fig. 6. Time dependence of ^{46}Sc production (solid curve) and the contribution of this production to the activity at recovery (dotted curve) for vanadium sample in Exp. P0006.

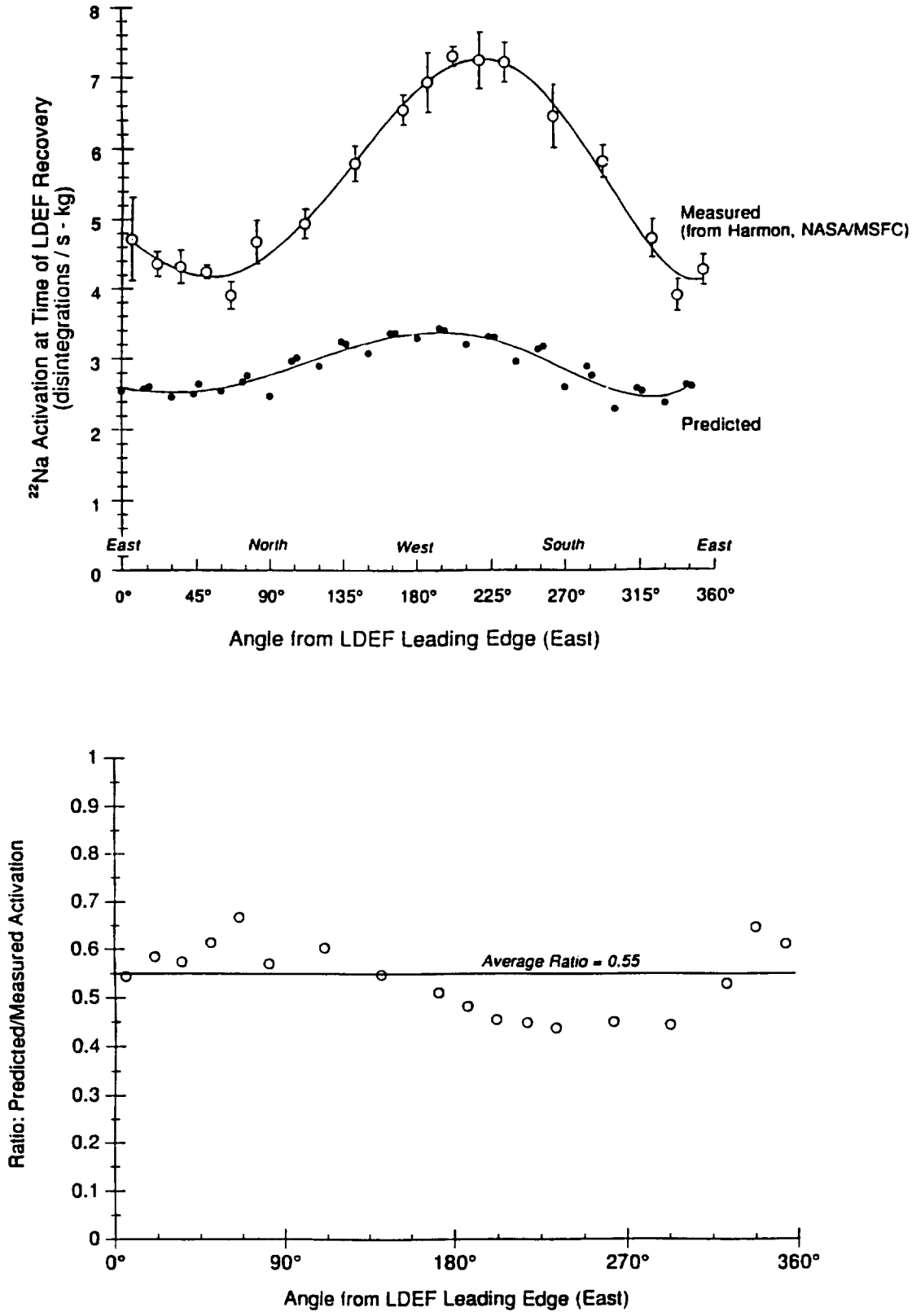

Fig. 7. Measured and predicted ^{22}Na activation of LDEF aluminum tray clamps (top), and predicted/measured ratio (bottom).

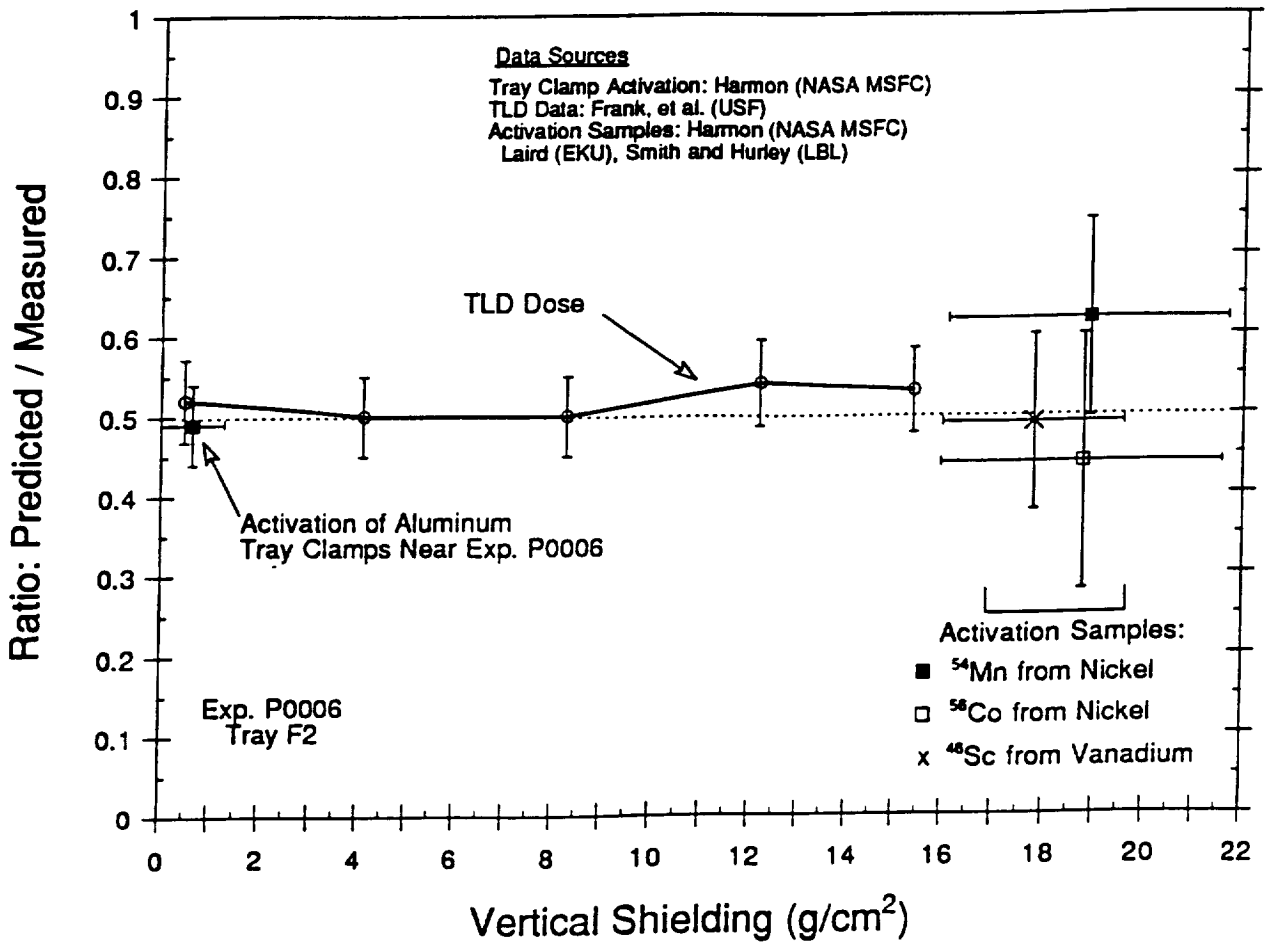

Fig. 8. Comparison of predicted vs. measured effects from trapped protons in LDEF experiment P0006 (Tray F2, trailing side).

Appendix B

Predictions of LET Spectra Measured on LDEF

Paper presented at Third LDEF Post-Retrieval Symposium
Published in NASA CP-3275 (1993)

PREDICTIONS OF LET SPECTRA MEASURED ON LDEF*

T. W. Armstrong and B. L. Colborn
Science Applications International Corporation**
Route 2, Prospect, TN 38477
Phone: 615/468-2603, Fax: 615/468-2676

E. V. Benton
Physics Research Laboratory, University of San Francisco**
2130 Fulton St., San Francisco, CA 94117-1080
Phone: 415/666-6281, Fax: 415/666/2469

ABSTRACT

The linear energy transfer (LET) spectra measured by plastic (CR-39) detectors in Exp. P0006 on LDEF are much higher at high LET than expected from methods commonly used to predict LET spectra produced by the space ionizing radiation environment. This discrepancy is being investigated by examining modeling approximations used in the predictions, and some interim results are presented.

INTRODUCTION

The P0006 Experiment on LDEF (ref. 1) contained plastic detectors (CR-39) for measuring linear energy transfer (LET) spectra. Analyses of these data reported to date, Benton, et al. (ref. 2), show observed spectra that are quite different than expected from commonly-used LET prediction methods. Since LET spectra are fundamental in predicting a variety of radiation effects of practical importance (e.g., biological damage, electronics upsets) in spacecraft and mission design, it is important to investigate the reason for this discrepancy, and reported here are some interim results of such work.

The problem addressed is illustrated by Fig. 1. Shown here is the measured LET spectrum (ref. 2) in one of the CR-39 sheets located 6.5 g/cm^2 from the space end of the main detector stack in the P0006 experiment. Also shown is a pre-recovery LET prediction made by Derrickson (ref. 3) using the NRL CREME code of Adams (ref. 4), which is commonly used for predicting LET spectra in performing assessments of space radiation effects on microelectronics. Since this pre-recovery prediction was of a scoping nature to

*Submitted for publication in Proceedings of Third LDEF Post-Retrieval Symposium: Williamsburg, Virginia, 8-12 Nov. 1993.

**Work supported by NASA Marshall Space Flight Center, Huntsville, Alabama.

obtain a quick estimate, several approximations were involved -- e.g.: (a) the spacecraft and detector shielding is approximated as an aluminum sphere, (b) the calculated LET spectra are for silicon, whereas the CR-39 data have been converted to LET in water, (c) the calculated spectra are for the space environment at the LDEF insertion altitude and not averaged over the LDEF mission, and (d) the calculation neglects the effects of secondary particles created in the detector and spacecraft, including both "projectile fragments" (secondaries from the breakup of incident ions during nuclear collisions) and "target fragments" (residual nuclei and secondary particles from collisions with detector material nuclei). Discussed below are calculations which remove some (but not all) of the approximations in the pre-recovery LET predictions.

LET PREDICTIONS

Shielding Effects

Since a detailed 3-D mass model of the LDEF spacecraft, experiment tray F2 contents containing the P0006 experiment, and the P0006 detector stack has been developed (ref. 5) for LDEF radiation analyses, the effects of shielding on the LET spectra predictions can be treated accurately. Therefore, the LET spectrum at a point in the center of the CR-39 layer corresponding to the location of the measured spectrum has been calculated using the LDEF 3-D shielding model. Radiation transport calculations were made for shielding in each of 720 solid angle bins around the detector point. A simplified representation of the shielding distribution is shown in Fig. 2. The transport calculations along each shielding direction were made using the Burrell transport code (ref. 6) for incident trapped protons and the CREME code (ref. 4) for galactic protons and heavy ions. The LDEF exposure to trapped protons predicted by Watts, et al. (ref. 7) was used, which takes into account the trapped proton anisotropy as well as altitude and solar cycle variations during the LDEF mission. Incident galactic cosmic ray spectra for the LDEF orbit were calculated using the CREME code. Average galactic spectra over LDEF altitude and solar cycle variations were computed, but the average results are not significantly different from the solar minimum spectra at the LDEF insertion altitude assumed in the pre-recovery predictions, as illustrated in Fig. 3 for protons. The LET spectrum in water is calculated to correspond to the data, as opposed to LET in silicon for the pre-recovery prediction of Fig. 1.

Results from this calculation are compared with measurements in Fig. 4. There is some improvement compared to Fig. 1 when shielding effects are taken into account, but the large difference for the high-LET "tail" ($\geq$ 1500 MeV $\cdot$ cm^2/g) still exists. The

difference at low LET (≤300 MeV · cm^2/g) is understandable because of the inherent insensitivity of CR-39 at low LET and because of the particular etching process used. Thus, the CR-39 has very low detection efficiency for trapped protons. This is illustrated in Fig. 5, which is the same as Fig. 4 but indicates the predicted trapped proton and galactic components.

SEP Iron Contribution

From measurements made by the HIIS experiment of Adams, et al. on LDEF, it was found that the large solar energetic particle (SEP) events during Oct. 1989 made a large contribution to the observed iron spectra in the energy range from ≈ 200-800 MeV/nucleon (ref. 8). Since iron ≥ 350 MeV/n can penetrate the 6.5 g/cm^2 minimum shielding of the CR-39 layer of interest in Exp. P0006, and since the LET calculations above neglect SEP events, we have checked the contribution of SEP iron to the LET.

These calculations were made by modifying the CREME code to incorporate the Fe spectra measured by HIIS on LDEF. LET spectra are compared in Fig. 6 with and without the SEP iron included. These results show that SEP iron makes some contribution at high LET, but not nearly enough to account for the predicted vs. observed discrepancy in Exp. P0006.

Contribution of Heavy Ion Fragmentation

To check the contribution at high LET from secondary particles generated when incident heavy ions breakup into lower-Z ions due to nuclear collisions, the UPROP code of Letaw (ref. 9) was used. This code accounts for the production and subsequent transport of all secondary particles from ion breakup in nuclear collisions. The results of this calculation (made for a spherical aluminum shield) show that, even for the case of rather thick shielding (50 g/cm^2), the secondaries from ion fragmentation do not significantly increase the LET spectrum (Fig. 7).

SUMMARY

The LET calculations described above remove some of the approximations made in initial, pre-recovery predictions, but they do not explain the large difference at high LET between predictions and measured spectra for Exp. P0006. The calculations to date have not taken into account target nuclei fragments and elastic recoils from nuclear collisions

produced by trapped protons, which is suspected as being the most likely cause of the large underprediction at high LET.

To account for the effects of nuclear interaction products from trapped proton collisions with the CR-39 constituents, a more detailed radiation transport calculation is required than possible with the codes used for the above predictions. A calculational approach for accurately simulating the CR-39 measurements is under development, but results are not yet available. The approach consists of two steps in the radiation transport: First, the trapped proton flux in the detector is computed using a standard proton transport code (e.g., ref. 6) and the 3-D LDEF spacecraft/detector model. This procedure, which has been used extensively for dose and activation predictions to compare with LDEF data (e.g., ref. 10), takes into account the trapped proton directionality and accurately treats shielding effects. In the second step, the proton flux in the CR-39 layer is used as the source for a 3-D Monte Carlo transport within the dosimeter. A modified version of the HETC code (ref. 11) can be used for the Monte Carlo calculation to take into account the production and transport of nuclear recoils and secondary particles in the detector region.

REFERENCES

1. Benton, Eugene V. and Parnell, Thomas A.: Linear Energy Transfer Spectrum Measurement Experiment (P0006): in The Long Duration Exposure Facility (LDEF) Mission 1 Experiments, Clark, Lenwood G. et al. (Eds), NASA SP-473, 1984.

2. Benton, E. V.; Csige, I.; Oda, K.; Henke, R. P.; Frank, A. L.; Benton, E. R.; Frigo, L.A.; Parnell, T. A.; Watts, J. W., Jr. and Derrickson, J. H.: LET Spectra Measurements of Charged Particles in the P0006 Experiment on LDEF, Second LDEF Post-Retrieval Symposium, NASA CP-3194, 1993.

3. Derrickson, J. H.: Linear Energy Transfer for the LDEF Mission: in Ionizing Radiation Exposure of LDEF (Pre-Recovery Estimates), E. V. Benton, et al. (Eds), *Nucl. Tracks Radiat. Meas.* 20, No. 1, 75 (1992).

4. Adams, James H., Jr.: Cosmic Ray Effects on Microelectronics, Part IV. NRL Memorandum Report 5901, December 1986.

5. Colborn, B. L. and Armstrong, T. W.: Development and Application of a 3-D Geometry/Mass Model for LDEF Satellite Ionizing Radiation Assessments. Second LDEF Post-Retrieval Symposium, NASA CP-3194, 1993.

6. Burrell, M.O.: The Calculation of Proton Penetration and Dose Rates. George C. Marshall Space Flight Center, Huntsville, AL., NASA TM X-53063, August 1964.

7. Watts, J. W., Jr.; Armstrong, T. W. and Colborn, B. L.: Revised Predictions of LDEF Exposure to Trapped Protons. Second LDEF Post-Retrieval Symposium, NASA CP-3194, 1993.

8. Adams, J. H., Jr.; Beahm, L. P.; Boberg, P. R.; Kleis, T. and Tylka, A. J.: HIIS Observations During the Large Energetic Particle Events of October 1989 (preprint).

9. Letaw, John R.: UPROP: A Heavy-Ion Propagation Code. Severn Communications Corp. Report SCC 89-02, August 1989.

10. Armstrong, T. W.; Colborn, B. L.; Harmon, B. A.; Parnell, T. A.; Watts, J. W., Jr. and Benton, E. V.: Comparison of Model Predictions with LDEF Satellite Radiation Measurements. *Adv. Space Res.* 14, No. 10, 17 (1994).

11. Armstrong, T. W. and Colborn, B. L.: A Thick-Target Radiation Transport Code for Low-Mass Heavy Ion Beams, HETC/LHI. *Nucl. Instr. Meth.* 169, 161 (1980).

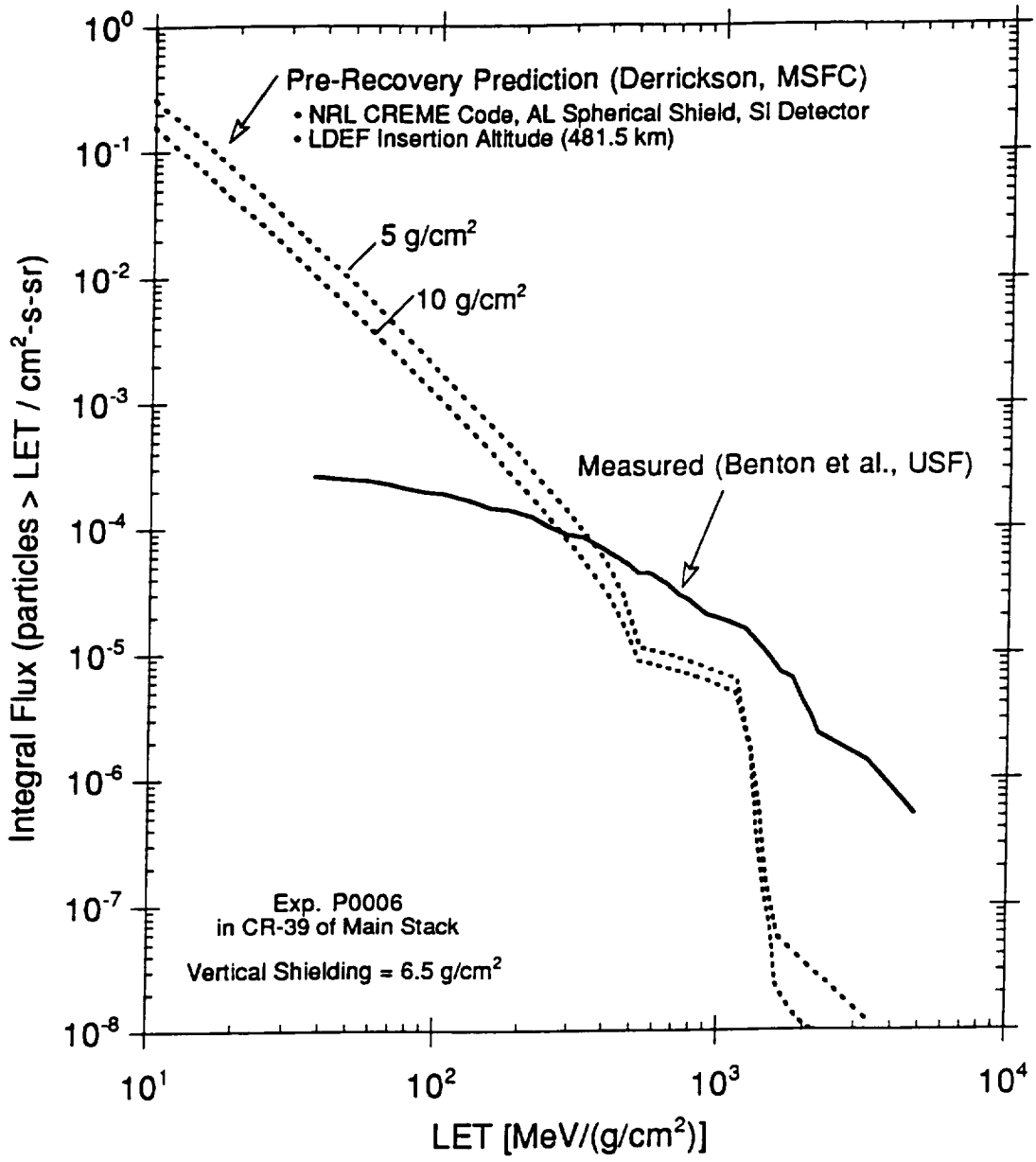

Fig. 1. Comparison of LET spectra measured (ref. 2) by LDEF Exp. P0006 plastic track detector with pre-recovery predictions (ref. 3).

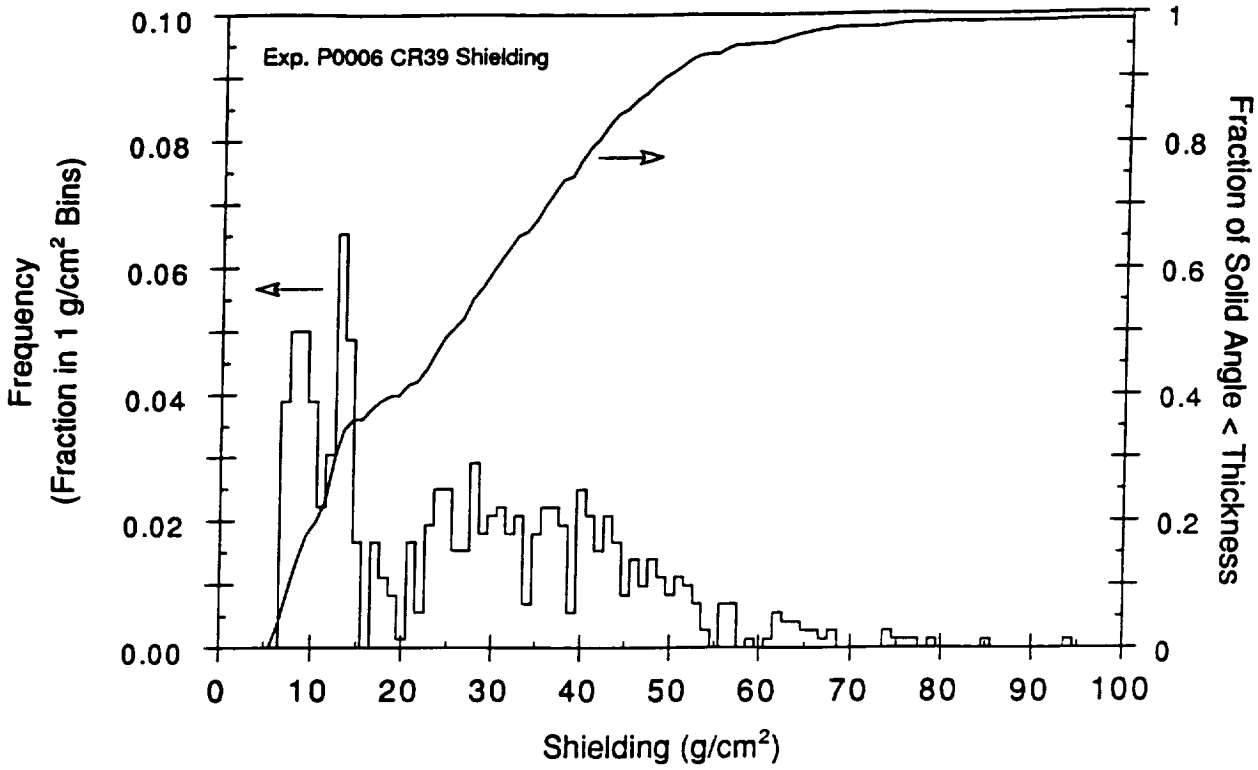

Fig. 2. Shielding distribution for P0006 detector.

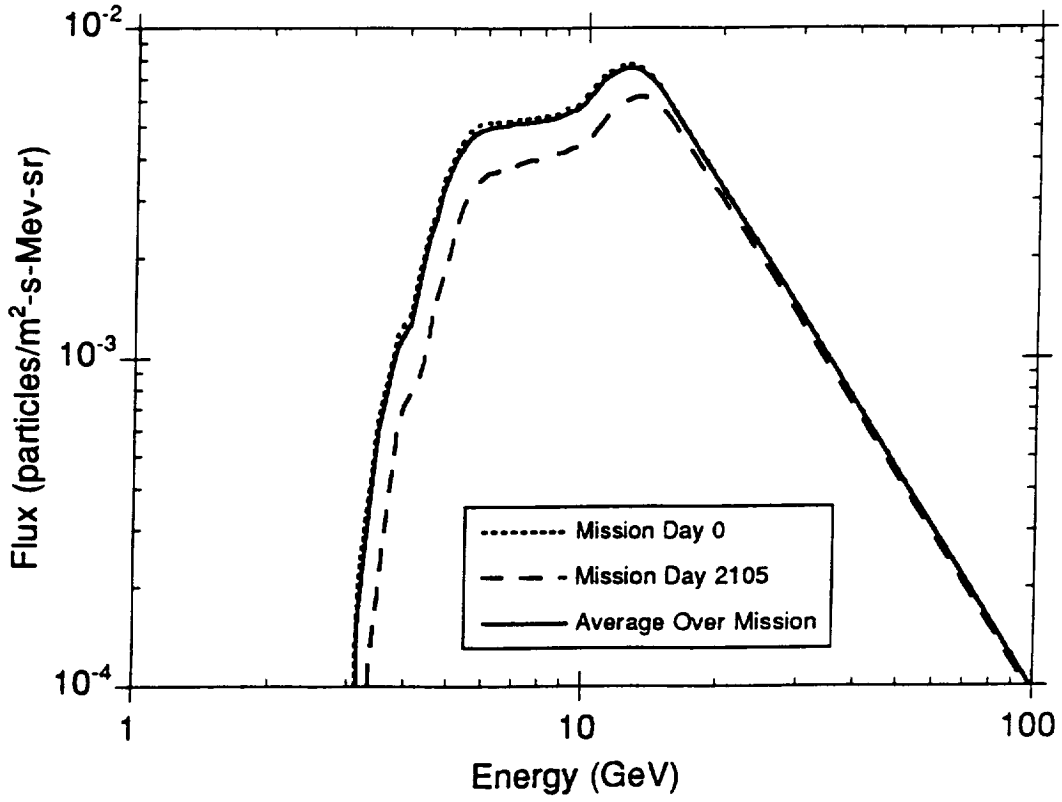

Fig. 3. LDEF exposure to galactic protons.

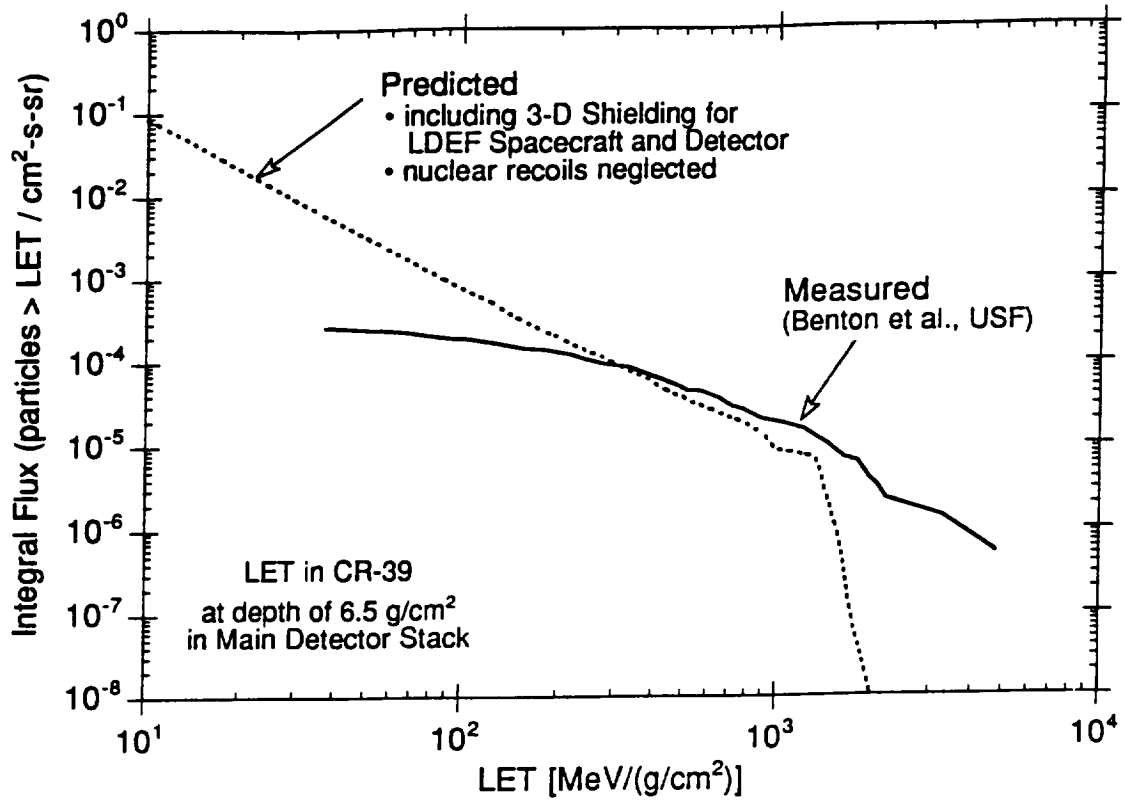

Fig. 4. Predicted LET using 3-D shielding model.

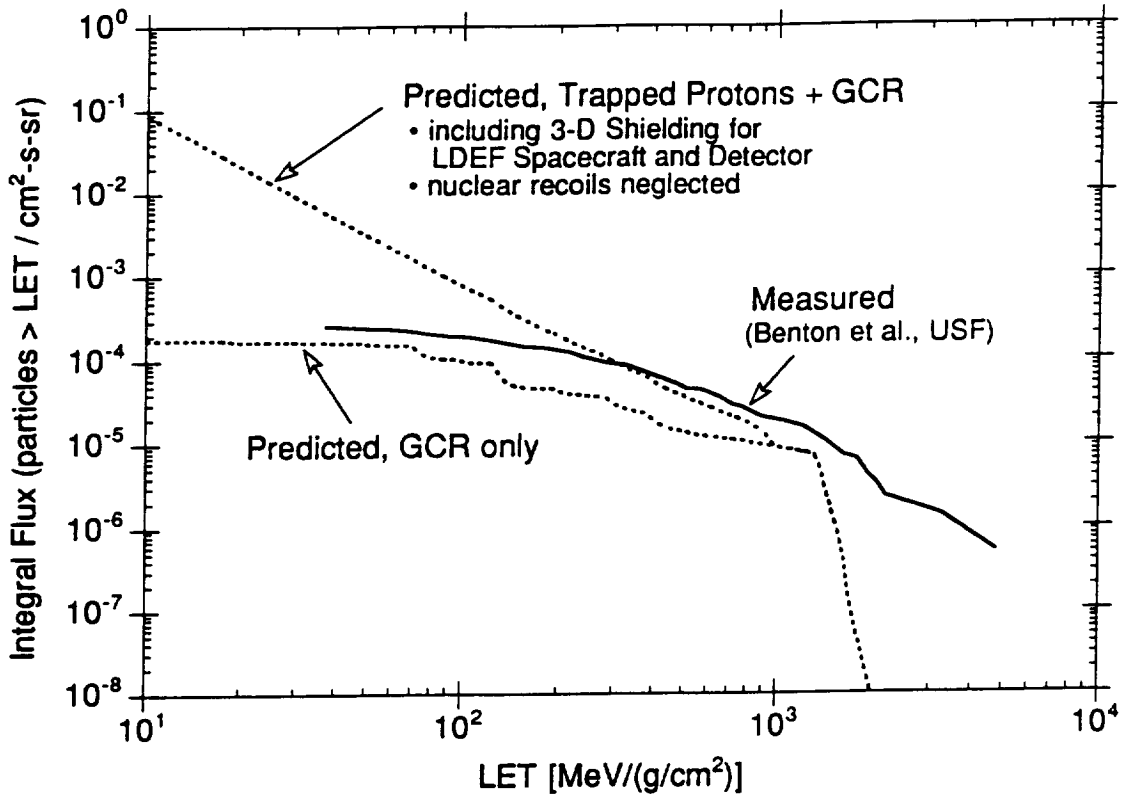

Fig. 5. Contribution of trapped protons to LET.

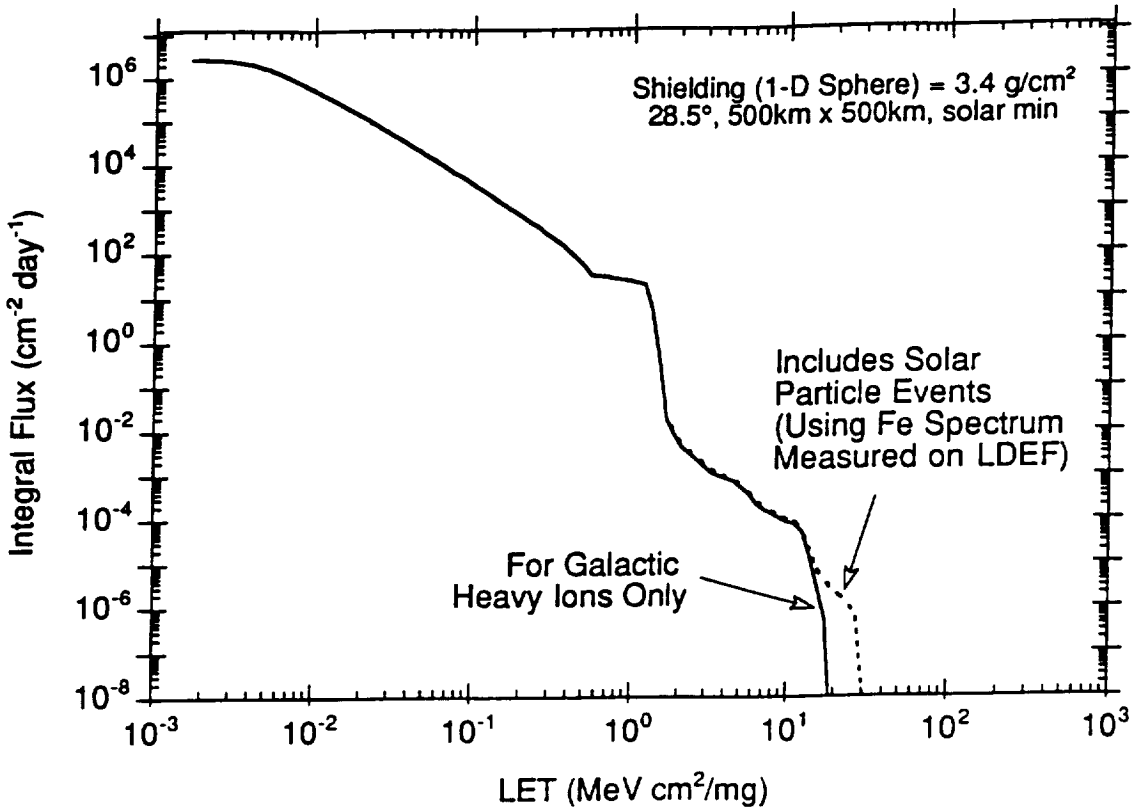

Fig. 6. Influence of SEP iron ions on LET.

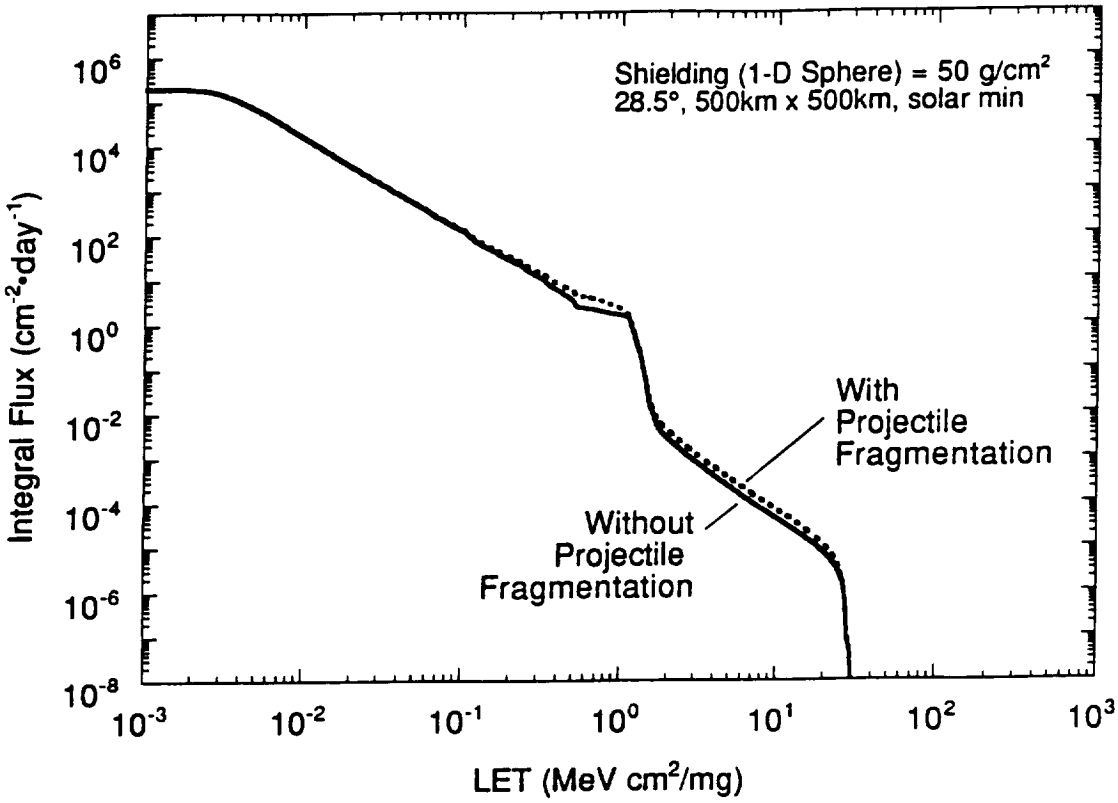

Fig. 7. Influence of ion ("projectile") fragmentation on LET.

REPORT DOCUMENTATION PAGE

Form Approved
OMB No. 0704-0188

Public reporting burden for this collection of information is estimated to average 1 hour per response, including the time for reviewing instructions, searching existing data sources, gathering and maintaining the data needed, and completing and reviewing the collection of information. Send comments regarding this burden estimate or any other aspect of this collection of information, including suggestions for reducing this burden to Washington Headquarters Services, Directorate for Information Operations and Reports, 1215 Jefferson Davis Highway, Suite 1204, Arlington, VA 22202-4302, and to the Office of Management and Budget, Paperwork Reduction Project (0704-0188), Washington, DC 20503

1. AGENCY USE ONLY (Leave blank)	2. REPORT DATE	3. REPORT TYPE AND DATES COVERED
	March 1996	Final Technical 5/92 - 12/95

4. TITLE AND SUBTITLE

LDEF Satellite Radiation Analyses

5. FUNDING NUMBERS

Contract No.
NAS8-39386

6. AUTHOR(S)

T. W. Armstrong and B. L. Colborn

7. PERFORMING ORGANIZATION NAME(S) AND ADDRESS(ES)

Science Applications International Corporation
Route 2
Prospect, TN 38477

8. PERFORMING ORGANIZATION REPORT NUMBER

SAIC-TN-96040

9. SPONSORING / MONITORING AGENCY NAME(S) AND ADDRESS(ES)

NASA Marshall Space Flight Center
Space Sciences Laboratory
Huntsville, AL 35812

10. SPONSORING / MONITORING AGENCY REPORT NUMBER

11. SUPPLEMENTARY NOTES

12a. DISTRIBUTION / AVAILABILITY STATEMENT

12b. DISTRIBUTION CODE

13. ABSTRACT *(Maximum 200 words).*

Model calculations and analyses have been carried out to compare with several sets of data (dose, induced radioactivity in various experiment samples and spacecraft components, fission foil measurements, and LET spectra) from passive radiation dosimetery on the Long Duration Exposure Facility (LDEF) satellite, which was recovered after almost six years in space. The calculations and data comparisons are used to estimate the accuracy of current models and methods for predicting the ionizing radiation environment in low earth orbit. The emphasis is on checking the accuracy of trapped proton flux and anisotropy models.

14. SUBJECT TERMS	15. NUMBER OF PAGES
LDEF satellite, ionizing radiation, environment models, trapped protons, trapped proton anisotropy, induced radioactivity, proton activation, LET spectra, radiation dose, AP8 model, AE8 model	55
	16. PRICE CODE

17. SECURITY CLASSIFICATION OF REPORT	18. SECURITY CLASSIFICATION OF THIS PAGE	19. SECURITY CLASSIFICATION OF ABSTRACT	20. LIMITATION OF ABSTRACT
UNCLASSIFIED	UNCLASSIFIED	UNCLASSIFIED	UL